

2015

## The Effect of Caffeine Supplementation on Muscular Power in Recreationally Trained College Aged Males

David John Sanders  
University of Rhode Island, dsanders7@yahoo.com

Follow this and additional works at: <https://digitalcommons.uri.edu/theses>

Terms of Use

All rights reserved under copyright.

---

### Recommended Citation

Sanders, David John, "The Effect of Caffeine Supplementation on Muscular Power in Recreationally Trained College Aged Males" (2015). *Open Access Master's Theses*. Paper 679.  
<https://digitalcommons.uri.edu/theses/679>

This Thesis is brought to you by the University of Rhode Island. It has been accepted for inclusion in Open Access Master's Theses by an authorized administrator of DigitalCommons@URI. For more information, please contact [digitalcommons-group@uri.edu](mailto:digitalcommons-group@uri.edu). For permission to reuse copyrighted content, contact the author directly.

RESISTIVITY METHODS APPLIED TO POLLUTION DETECTION  
IN A CRYSTALLINE BEDROCK AQUIFER  
AT LITTLE COMPTON, R.I.

BY  
DAVID PATRICK SANDERS

A THESIS SUBMITTED IN PARTIAL FULFILLMENT OF THE  
REQUIREMENTS FOR THE DEGREE OF  
MASTER OF SCIENCE  
IN  
GEOLOGY

UNIVERSITY OF RHODE ISLAND

1983

## ABSTRACT

Surface methods of electrical resistivity measurement are used to detect a layer of salt-polluted groundwater within a crystalline bedrock aquifer. Fractured, schistose bedrock overlain by a 15ft (4.6m) thickness of jointed till has been polluted by runoff from a storage facility for road salt in Little Compton, Rhode Island. Conductivity measurements in two bedrock monitoring wells on the site confirm the existence of highly mineralized groundwater in the bedrock aquifer. Interpretations of two vertical electrical sounding (VES) curves obtained slightly up-gradient topographically from the pollution source show that a 160-177ft (49-54m) thickness of bedrock is polluted while the entire thickness of till is relatively unpolluted. Interpretations of four other VES curves obtained slightly down-gradient from the pollution source show that the till layer is polluted, but the polluted bedrock layer is undetectable. Where the till is polluted, the till's bulk resistivity apparently is sufficiently reduced to suppress the effect of a polluted bedrock layer. While the suppression phenomenon is a major obstacle to the use of resistivity methods in areas of surficial pollution, in outlying areas where high concentrations of mineralized groundwater have flowed more rapidly through the bedrock aquifer than through the surficial aquifer, resistivity methods may be more efficient than random drilling for

detecting bedrock pollution. The bulk resistivities interpreted for polluted bedrock compare favorably with published laboratory measurements on rock samples. A calculated bedrock formation factor of 77 is used in conjunction with Archie's law to obtain a quantitative measure of the pollution. Two other resistivity methods, horizontal profiling and AB rectangle mapping, did not provide conclusive evidence of bedrock pollution where the overlying till was also polluted. However, an AB rectangle map over unpolluted till shows a resistivity contour pattern similar to the fracture orientation observed in local bedrock outcrops. With further research and the development of a computer program to perform the numerous calculations, the AB rectangle method could prove to be an effective method for the placement of bedrock monitoring wells.

**ACKNOWLEDGEMENTS**

The guidance given the author by Professors R. K. Frohlich, J. J. Fisher, and V. A. Nacci during the preparation of this thesis are greatly appreciated. The author is grateful for the field assistance of R. Kowalski, T. Pac, C. Parke, and D. Hazebrouck. The R. I. Department of Transportation and the residents neighboring the Little Compton State Garage are recognized for allowing access to the site. A summer research assistantship awarded the author by Professor W. E. Kelly through the R. I. Water Resources Center is acknowledged as are the helpful discussions with Professor D. W. Urish. The author must also acknowledge Professor D. S. Snipes of Clemson University and Mr. B. C. Spigner of Soil and Material Engineers Inc., Columbia, S. C. for encouraging the pursuit of this degree. Lastly, only with the support of my parents has the completion of this thesis been possible.

TABLE OF CONTENTS

ABSTRACT.....ii

ACKNOWLEDGEMENTS.....iv

LIST OF TABLES.....vii

LIST OF FIGURES.....viii

INTRODUCTION.....1

RESISTIVITY METHOD FOR INVESTIGATING AQUIFER POLLUTION.....4

    Introduction to the Resistivity Method.....4

    Horizontal Profiles.....9

    Vertical Electrical Soundings.....11

        General procedure.....11

        VES curve interpretation and nonuniqueness.....17

        Formation factor and Archie's law.....22

    AB Rectangles.....26

HYDROGEOLOGY OF FRACTURED CRYSTALLINE BEDROCK.....31

    Crystalline Bedrock as an Aquifer.....31

    Fracture Types and Their Relation to Groundwater.....32

    Porosities of Crystalline Bedrock Aquifers.....35

    Pollutant Flow in Crystalline Bedrock Aquifers.....38

    Geology and Hydrogeology at Little Compton, R-I.....42

ANALYSIS OF RESISTIVITY IN CRYSTALLINE BEDROCK.....51

    Need for Field Research.....51

    Previous Studies on Rock Samples.....53

FIELD RESEARCH AT LITTLE COMPTON, R.I.....	59
Horizontal Profiling.....	59
Instrumentation and measurement locations.....	59
Discussion of results.....	62
Vertical Electrical Sounding.....	63
Instrumentation and measurement locations.....	63
Discussion of results.....	66
Application of formation factor and Archie's law.....	82
AB Rectangle Mapping.....	87
Instrumentation and measurement locations.....	87
Discussion of results.....	93
SUMMARY.....	97
REFERENCES CITED.....	99
APPENDIX A. Fortran Program for Computing K-factors.....	106
APPENDIX B. Horizontal Profiling Field Data.....	107
APPENDIX C. Vertical Electrical Sounding Field Data.....	108
APPENDIX D. AB Rectangle Mapping Field Data.....	115

## LIST OF TABLES

Table 1.	Borehole measurements.....	65
Table 2.	Field Data for W to E Horizontal Profile Line..	107
Table 3.	Field Data for N to S Horizontal Profile Line..	107
Table 4.	Field Data for VES 1.....	108
Table 5.	Field Data for VES 2.....	109
Table 6.	Field Data for VES 3.....	109
Table 7.	Field Data for VES 4.....	110
Table 8.	Field Data for VES 5.....	112
Table 9.	Field Data for VES 6.....	113
Table 10.	Field Data for ABR 1.....	115
Table 11.	Field Data for ABR 2.....	116
Table 12.	Field Data for ABR 3.....	118
Table 13.	Field Data for ABR 4.....	119



## LIST OF FIGURES

Figure 1.	Location of the Little Compton site.....	3
Figure 2.	Electrode configurations for resistivity measurements.....	6
Figure 3.	Generalized graphs of VES curves.....	13
Figure 4.	VES oriented perpendicular to the elongation of a plume.....	20
Figure 5.	AB rectangle calculations.....	28
Figure 6.	Bedrock geology at Little Compton.....	45
Figure 7.	Location map of horizontal profiles.....	60
Figure 8.	Graph of horizontal profiling resistivities versus distance.....	61
Figure 9.	Location map of VES center points.....	67
Figure 10.	Field curve and geoelectric model for VES 1....	68
Figure 11.	Field curve and geoelectric model for VES 2....	69
Figure 12.	Field curve and geoelectric model for VES 3....	70
Figure 13.	Field curve and geoelectric model for VES 4....	71
Figure 14.	Field curve and geoelectric model for VES 5....	72
Figure 15.	Field curve and geoelectric model for VES 6....	73
Figure 16.	Theoretical models of third-layer suppression..	81
Figure 17.	Location map of AB Rectangles.....	88
Figure 18.	Resistivity contour map for ABR 1.....	89
Figure 19.	Resistivity contour map for ABR 2.....	90
Figure 20.	Resistivity contour map for ABR 3.....	91
Figure 21.	Resistivity contour map for ABR 4.....	92

## INTRODUCTION

Investigations of groundwater pollution in Rhode Island and elsewhere are often limited to surficial aquifers in unconsolidated sediments. Perhaps equally, if not more, important at some sites is the flow of pollutants through the underlying fractured bedrock aquifer. Subsurface conditions can be such that polluted groundwater flows from the surficial aquifer into fractures in the bedrock. If the fractures are sufficiently interconnected, the pollutants may travel at a faster rate and at higher concentrations through the fracture network than through the surficial aquifer. Thus, pollution in a bedrock aquifer can be more of a threat than pollution in a surficial aquifer to wells that tap both. From an investigative viewpoint the flow of pollutants in a bedrock aquifer tends to be less predictable and more difficult to monitor than the flow of pollutants in a surficial aquifer. This is due to the irregular distribution of void spaces in fractured bedrock and the large scale at which permeability must be considered. With a greater public awareness of the high susceptibility of bedrock wells to groundwater pollution will come a greater demand for methods to investigate this intriguing hydrogeologic problem.

During the summer of 1982, the author and a co-worker initiated research into the flow of pollutants through fractured crystalline bedrock (Kowalski and Sanders, 1983).

As a part of this research, some preliminary electrical resistivity measurements were made at the Rhode Island Department of Transportation State Garage in Little Compton. This facility in southeastern Rhode Island (figure 1) is the town's storage site for road salt which is mixed with sand and used during the winter months for deicing roadways. A report by Kelly and Urish (1981) noted significant amounts of dissolved salt were draining from the site and causing contamination of the groundwater. In conjunction with this report, two shallow bedrock monitoring wells (boreholes) were installed at the site, both of which have indicated sodium chloride pollution in the bedrock aquifer. The resistivity measurements made in 1982 also suggested the presence of mineralized groundwater surrounding the site. More resistivity measurements were made in April 1983, the results of which are presented here.

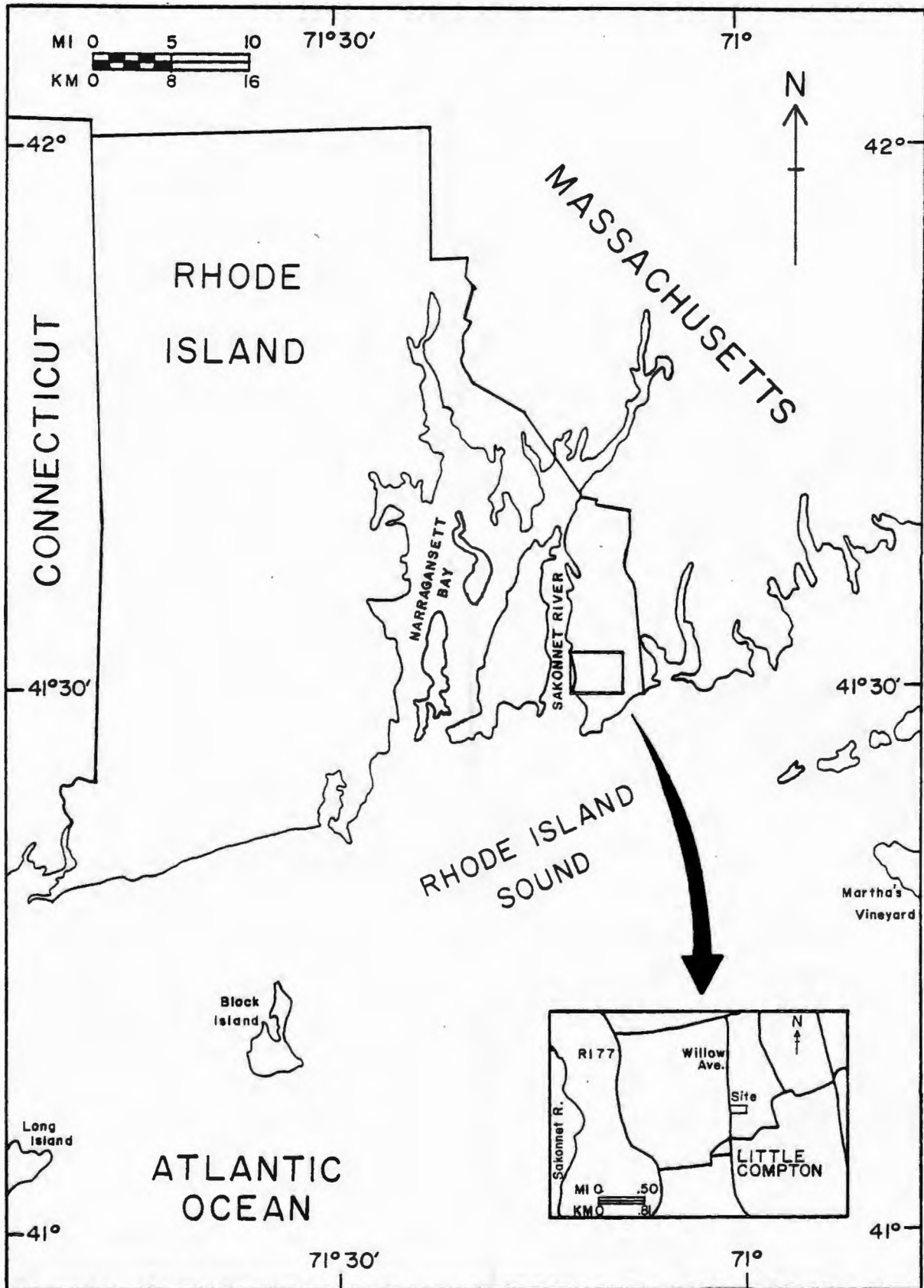


Figure 1. Location of the Little Compton site

## RESISTIVITY METHOD FOR INVESTIGATING AQUIFER POLLUTION

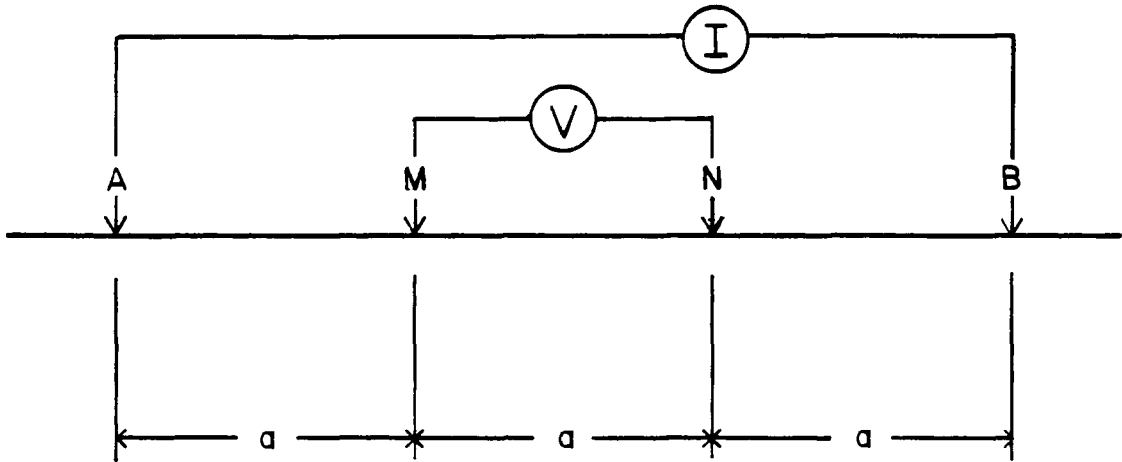
### Introduction to the Resistivity Method

No other physical property of earth materials can display a wider range of values than electrical resistivity (Van Nostrand and Cook, 1966; Zohdy et al, 1974). Within the past century, a surface geophysical method has been developed that utilizes the variation in resistivity from one buried medium to another in order to prospect for ore deposits and fluid-bearing formations. This method, the resistivity method, has been applied to groundwater exploration since World War II (Breusse, 1963) and much has been published to document its validity. More recently, two versions of the resistivity method, horizontal profiling and vertical electrical sounding (VES), have been employed to locate and trace the movement of polluted groundwater from waste disposal sites (Warner, 1969; Stollar and Roux, 1975; Kelly, 1976; Urish, 1983).

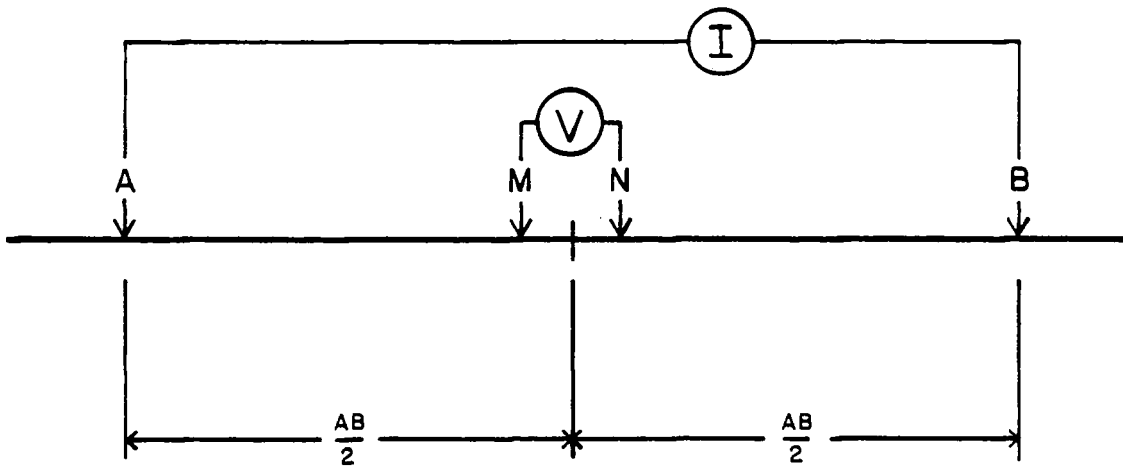
Polluted groundwater from waste disposal sites, as well as from salt storage sites, commonly contains higher concentrations of ions in solution than the natural groundwater surrounding the site. This increases the electrolytic conduction of electrical current through the polluted groundwater. A direct electrical current can be

conducted through a possibly contaminated subsurface through two electrodes at the ground surface. With a measure of the current and of the potential difference between two additional colinear electrodes, the resistivity of the subsurface can be calculated. If it can be determined that lateral inhomogeneities in the subsurface matrix material are not causing the variations in resistivity from one measuring point to another (Klefstad et al, 1975), the variations in resistivity can be ascribed to effects of groundwater pollution. Therefore, a low resistivity value at a measuring point implies that the subsurface below that point contains high conductivity polluted groundwater. In this way areas of groundwater pollution can be delineated by horizontal profiling or by another method to be introduced, namely the AB rectangle method. Depths and layers of pollution can be interpreted from vertical electrical soundings.

Two of the most commonly used electrode configurations are the Wenner array (figure 2a) and the Schlumberger array (figure 2b). For both configurations, the outer two electrodes (A and B) deliver the current while the inner two electrodes (M and N) measure the potential difference. The difference between the two configurations is their spacing between potential electrodes. For the Wenner array, the separation between all four electrodes is equal and is referred to as the a-spacing. For the Schlumberger array, the current electrode separation is always at least five



a. Wenner array



b. Schlumberger array

Figure 2. Electrode configurations for resistivity measurements

times greater than the potential electrode separation. Since the distance between potential electrodes in the Schlumberger array is smaller than for the Wenner array at the same current electrode separation, the potential difference (voltage drop) for the same current is also smaller. This is usually cited as a disadvantage of the Schlumberger array because a smaller value is sometimes measured less precisely than a larger one. However, the smaller distance over which the voltage gradient is measured tends to diminish effects from lateral inhomogeneities which is seen as an advantage of the Schlumberger array. The disadvantage of measuring smaller voltages is overcome by the higher precision of modern measuring instruments.

Most subsurfaces consist of more than one geoelectric layer. A boundary between two geoelectric layers is defined by a change in bulk resistivity, which is the combined resistive effect of the rock matrix and the material that fills the void spaces. A change in bulk resistivity, therefore, may be caused by a change in the shape and distribution of the void spaces in the rock matrix. This would likely result from a difference in lithology between the two geoelectric layers. A change in bulk resistivity may also be caused by a change in the saturation of the void spaces or in the quality of the water in the void spaces. Note, however, that the difference in bulk resistivity between two layers is seldom attributable to a change in the resistivity of the rock matrix itself. In effect, the bulk



resistivity of a saturated layer is controlled by the distribution and the quality of the water occupying the void spaces (Zohdy et al, 1974).

The bulk resistivity of a geoelectric layer is sometimes referred to as the true resistivity of a layer or simply as the layer resistivity ( $R_i$ ). When a resistivity measurement is taken, the resistivity value that is calculated is actually a weighted average of the true resistivities of each geoelectric layer that the current encounters. A resistivity value calculated from measurements at the ground surface is therefore properly termed an apparent resistivity ( $R_a$ ).

The general formula for calculating the apparent resistivity in ohm-feet (or ohm-meters) of a horizontally layered subsurface is

$$R_a = K V / I \quad (1)$$

where the geometric factor ( $K$ ) is measured in feet (or meters), the potential difference ( $V$ ) is measured in millivolts, and the direct current is measured in milliamperes. Referring to figure 2, the apparent resistivity for the Wenner array is calculated for each measurement by

$$R_a = (6.28 V / I) a \quad (2)$$

The apparent resistivity for the Schlumberger array is calculated by

$$R_a = (3.14 V / I) \frac{(AB/2)^2 + (MN/2)^2}{MN} \quad (3)$$

The value of apparent resistivity is usually assigned to the geometric center of the electrode configuration.

### Horizontal Profiles

Lateral variations in apparent resistivity can be detected using the horizontal profiling method. If two or more horizontal profiles are performed parallel to each other, a map of the areal variation in apparent resistivity can be prepared. In horizontal profiling the equal spacing between all four electrodes of the Wenner array (a-spacing) is kept constant as the whole array is displaced for each measurement. In practice when all the electrodes are of the same type, only the trailing electrode needs to be "leap-frogged" to the forward position as the array is moved down a line. Of course, the cable connections must be shifted accordingly for each measurement so that the current will be passing through the correct electrodes. In this way the apparent resistivity at the center point of each array position can be calculated by equation 2.

If other lateral inhomogeneities in the subsurface are insignificant, the lateral inhomogeneity produced by the

variation in groundwater resistivity due to pollution will cause the variation of apparent resistivity along the profile. For a single horizontal profile, the distance of each center point from the original center point is plotted versus the corresponding apparent resistivity on a graph. For several parallel profiles, each apparent resistivity is plotted on a map of the area at the location of the center point. Contour lines are drawn connecting points of equal resistivity. Positions of lower resistivity on either the graph or the map indicate zones of more-mineralized groundwater.

Zohdy et al (1974) recommend that at least two different a-spacings should be used in making horizontal profiles. Preferably, the values for the constant a-spacings are obtained from vertical electrical soundings along the profile line. Several a-spacings are chosen on the basis of the current electrode separation needed to penetrate a desired depth (Kowalski and Sanders, 1983). In an ideal laterally homogeneous subsurface, a certain a-spacing will yield apparent resistivity values from a constant depth, or more precisely a constant range of depths that optimally contributes to the apparent resistivity measured. However, at pollution sites the very inhomogeneity that is to be measured - the lateral variation of groundwater resistivity - will cause a change in the depth range that is contributing. It therefore can be stated that the greater the variation of apparent

resistivity is along a profile line, the greater the variation of probing depth will be. As can be seen, horizontal profiling is generally a qualitative method from which only trends in the pollution pattern can be discerned.

## Vertical Electrical Soundings

### General procedure

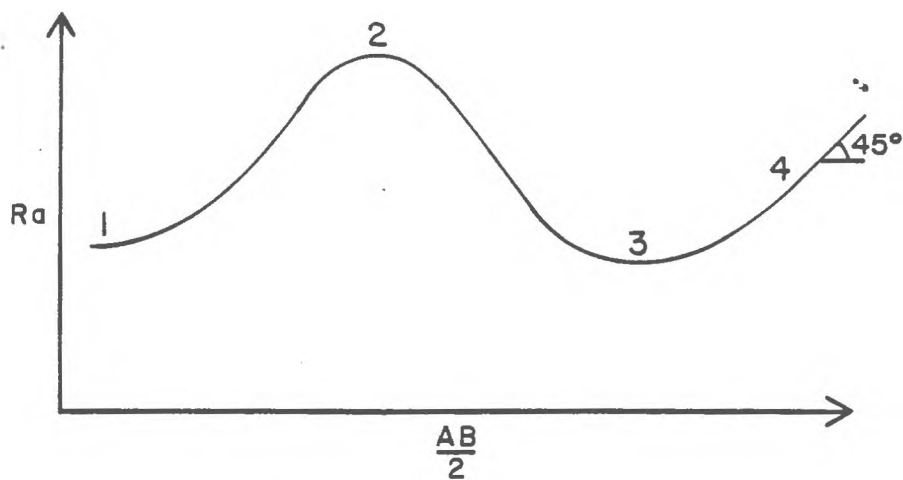
Vertical electrical soundings are performed over a stationary center point by systematically increasing the distance between current electrodes along a line. Apparent resistivity measurements are taken at successive logarithmic intervals of current electrode separation. This results in a depth investigation from which the various geoelectric layer thicknesses and resistivities can be modeled. The basis for VES interpretation is that as the current electrode separation is increased, the probing depth will be greater. Zohdy et al (1974) point out that the increased probing depth is actually caused by the increased distance between current and potential electrodes.

The Schlumberger array is most frequently used for performing vertical electrical soundings. As the current electrodes are moved outward it is not necessary to move the potential electrodes until their spacing is 1/20 to 1/50 the

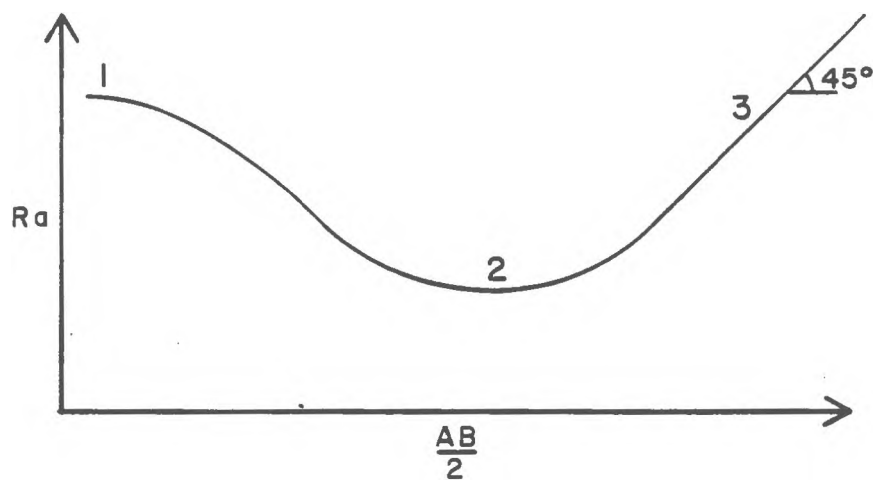
spacing of the current electrodes (Koefoed, 1979). This assumes that somewhere between these electrode ratios, the potential difference will become so small that it can no longer be measured due to the resolution of the measuring instrument (voltmeter). Also, natural variations in the electrical field of the subsurface may produce noise that can interfere with the precise measurement of low voltages. When this happens the potential electrodes can be displaced outward from the center point so that measurements of larger values can be made. Measurements are made at both the old and the new potential electrode spacings while the current electrode spacing is kept constant. This allows for the adjustment of successive measurements if necessary during the interpretation process.

The various apparent resistivities calculated by equation 3 in the field are plotted for each current electrode interval of a VES on a bilogarithmic graph. The half-electrode separation ( $AB/2$ ) is measured along the abscissa while the apparent resistivity is measured along the ordinate. The plot of all the apparent resistivities yields as VES curve with one or more maxima and/or minima from which the subsurface geoelectric layering can be interpreted.

Figure 3 shows generalized graphs of the two types of curves encountered at Little Compton. The portions of the two curves denoted by the number 1 asymptotically approach to the left apparent resistivity and  $AB/2$  values that are



a. KH-type VES Curve



b. H-type VES Curve

Figure 3. Generalized graphs of VES curves

respectively the first layer bulk resistivity and thickness. The curve reaches a local maximum at number 2 in figure 3a because layer 2 has a higher bulk resistivity than layer 1. Likewise in figure 3b a minimum is reached at number 2 because layer 2, in this case, has a lower bulk resistivity than layer 1. Figure 3a shows a third layer of finite resistivity and thickness as indicated by the minimum at number 3. It can be seen from figure 3a that the bulk resistivities of layers 2 and 4 ( $R_2$  and  $R_4$ ) are higher than those of layers 1 and 3 ( $R_1$  and  $R_3$ ). When  $R_1 < R_2 > R_3 < R_4$ , the curve is called a KH-type curve. When  $R_1 > R_2 < R_3$ , the curve is called an H-type curve (figure 3b). Both curves eventually rise at an angle of  $45^\circ$  meaning a layer of relatively infinite resistivity has been reached (number 4 on figure 3a, number 3 on figure 3b). In most resistivity interpretations this nonconductive layer is identified as bedrock and the sum of the thicknesses above it are considered to be the depth to the bedrock surface. Exceptions to this interpretation are of importance later.

The general procedure for detecting aquifer pollution from a Schlumberger VES curve is outlined below and is discussed further in the paragraphs that follow.

Step 1: Apparent resistivities ( $R_a$ ) are calculated from measured values of current, potential difference, and electrode spacings using equation 3 above. A plot of  $R_a$  versus  $AB/2$  on logarithmic scales comprises a VES field curve.

Step 2: A geoelectric model of layer thicknesses and layer resistivities that correlates with the observed curve and any known depths to geologic / hydrogeologic layers is obtained through curve-matching and computer analysis. The theoretical curve generated by this model is based on a horizontally layered subsurface. Subsequently, a uniform value of thickness and bulk resistivity is assigned to each layer in order to approximate the actual subsurface situation.

Step 3: From the geoelectric models obtained by steps 1 and 2 for each field curve at the polluted site, the layer that represents the polluted aquifer of interest is identified. The range of practically equivalent values of bulk resistivity and thickness for the chosen layer in each geoelectric model is determined from a published nomogram.

Step 4: Since the bulk resistivity of a layer is dependent on the structure of the rock matrix and the amount and quality of the saturating groundwater, relationships can be used to estimate unknown values from known values. The ratio of bulk resistivity to groundwater resistivity, called the formation factor (equation 4 below), has been shown empirically to be nearly constant for a layer with both a highly-mineralized saturating fluid and a homogeneous rock matrix. The formation factor is related to porosity and to two rock matrix factors by an empirical formula known as



Archie's law (equation 6 below). If a measure of the groundwater conductivity from a borehole near a VES center point is available, the modeled layer resistivity can be used to calculate the formation factor. With this number, the groundwater conductivity (inverse resistivity) can be estimated at other VES locations by substituting their respective modeled layer resistivities into the equation. From the derived variations in groundwater conductivity, qualitative assessments can be made of the degree of pollution at each VES location. Quantitative assessments can be made if a conductivity of the natural groundwater is known or if the temperature of the groundwater is measured and used to approximate salinities from published nomograms. With a known formation factor value and a suitable expression of Archie's law, the total porosity of the layer of interest can be estimated. The porosity value can then be used to calculate a rough estimate of the rate of pollution movement through the layer (equation 7 below).

## VES curve interpretation and nonuniqueness

VES curves are first interpreted using two-layer master curves and auxiliary point diagrams. Published master-curves are widely available and the curve matching procedure is described in many resistivity texts (Keller and Frischknecht, 1966; Bhattacharya and Patra, 1968). Once a preliminary geoelectric model is developed for a VES curve, it can be slightly modified to correspond to known depths from a borehole by adjusting the layer thicknesses. When a layer thickness of an H-type curve model is increased or decreased, the layer resistivity must be increased or decreased accordingly to insure the ratio of thickness to resistivity, which is called the longitudinal conductance (S), stays constant. The total longitudinal conductance or the sum of S for all the finite resistivity layers controls the position of the 45° line at the end of certain curves including all the curves from Little Compton. Total S can be quickly calculated by dividing any AB/2 value of a point on the 45° line by its corresponding apparent resistivity value.

The task of modifying layer thicknesses and resistivities to produce a curve that closely fits the measured points has been made easier within the past few years by the accessibility of computers. A computer program from Koefoed (1979) that uses the linear filter method generated points on the Little Compton curves for

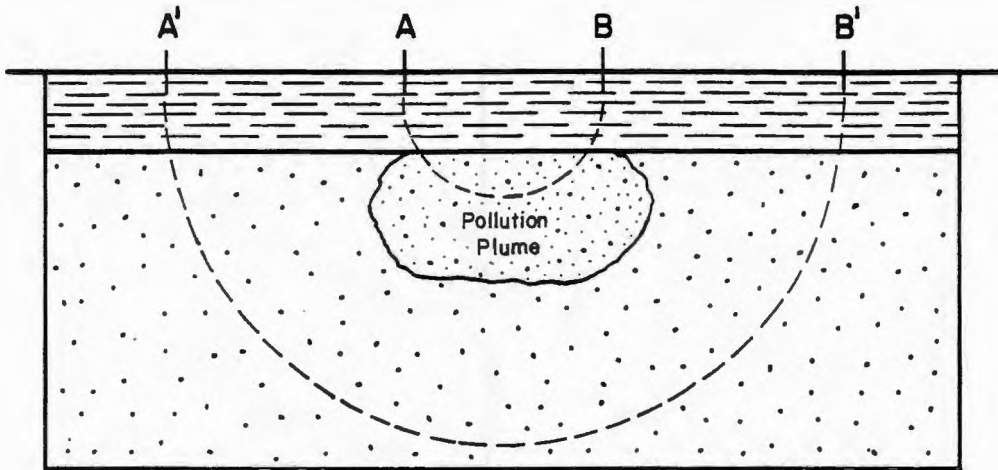
each geoelectric model that was tried. Modifications of the preliminary curve-matching model were entered into the program on a desk-top computer. By keeping  $S$  nearly constant, assuring that the  $45^\circ$  line does not shift from where it should be on the curve, and by forcing the known thicknesses from the borehole (depth to static water level, depth to bedrock) into various geoelectric models, curve points were generated until the best fit of a theoretical curve to the observed curve was obtained.

Whether a theoretical curve appears to fit the observed data or not is somewhat subjective. Quantitatively, if it is assumed that the maximum error in making the field measurements is  $\pm 5\%$  (Bhattacharya and Patra, 1968), it is possible to have significantly different model interpretations yield curves that appear to be practically coincident to the observed curve or, in other words, within 5% above and below the observed curve. The coincidence of curves is explained by the principle of equivalence. Two geoelectric models are said to be practically equivalent if their curves appear to practically coincide (Zohdy et al, 1974). There are limiting values for the second layer thickness and resistivity beyond which the principle of equivalence is no longer valid. Bhattacharya and Patra (1968) present Pylaev's nomograms for determining these limits.

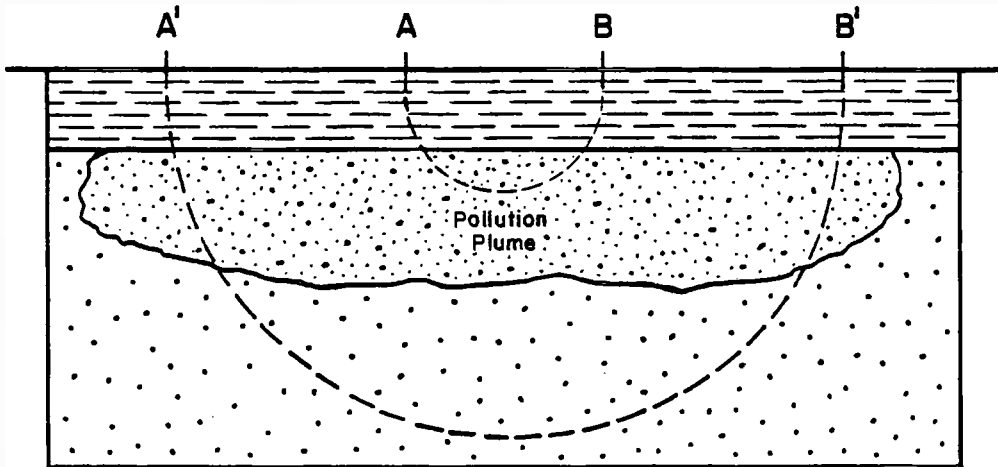
There are several reasons why some best-fitted theoretical curves may vary from the observed by more than

the 5% attributable to field measurement error. Lateral inhomogeneities in the subsurface encountered by the current as the current electrode spacing is expanded may cause humps or dips that cannot be fitted with simple three or four-layer curves. An example would be a local concentration of large boulders in a layer of till away from the center point of a VES which is only encountered at large  $AB/2$ . A more likely inhomogeneity in a polluted subsurface, however, would be a lateral change in the groundwater resistivity along a VES line. Since a plume of pollution tends to elongate in the direction of groundwater flow, a VES line centered over the plume and oriented perpendicular to the elongation may overrun the plume at large  $AB/2$  (figure 4a). This could cause a narrow plume at depth to be undetectable as a minimum on the observed curve. However, a plume that has a large width relative to depth (figure 4b) will probably show a minimum on the curve even though an anomalous rise in the curve may appear especially on the larger  $AB/2$  side of the minimum. While interpreting such a case, it is more practical to simply ignore the anomaly and fit the theoretical curve as if the observed curve were smooth, rather than try to add a nonexistent layer or layers to make a closer fit.

In considering the effect of overrunning a pollution plume, it should be noted that the pollution zone is not likely to end abruptly, but rather gradually decrease in concentration over some distance. If the zone of transition



a. Cross-section of some electrical current paths through an undetectable plume



b. Cross-section of some electrical current paths through a detectable plume

Figure 4. VES oriented perpendicular to the elongation of a plume

between low resistivity polluted groundwater and higher resistivity unpolluted groundwater is large enough especially beneath the plume, it can be modeled as one or more homogeneous layers of intermediate resistivity (Unz, 1968). At the margin of a plume the contact between a polluted layer and an unpolluted layer may dip away from the pollution source. However, Unz (1953) states contacts that dip at an angle of less than  $10^\circ$  may be modeled simply as a horizontal case.

Another reason for the lack of a close fit between a theoretical curve and a portion of an observed curve may be that the layering of the model has been oversimplified, meaning that one or more layers would have to be added before a better fit could be obtained. A complicated layering, however, further complicates the correlation of a geoelectric model with other geoelectric models in the vicinity. Without having a more detailed geologic section, it would be desirable to keep the interpretations generalized because of the equivalence problem. In other words, unless more layer thicknesses or resistivities are known, any interpretation that is developed for a complicated layering may be nonunique. Practically equivalent models could be produced and no evidence would be available to reject any of them.

With this in mind, however, there may be subsurface information available that would support the addition of a layer to a geoelectric model which would produce a

practically coincident curve. The principle of suppression explains why a layer may not influence the shape of a curve even though it has a distinct contrast in resistivity from its neighboring layers. For example, if  $R_1 < R_2 < R_3$ , layer 2 may happen to have a thickness and a resistivity that causes it to be masked by the thicknesses and resistivities of the overlying layers. As will be seen later, this nonuniqueness problem is relevant to the Little Compton site.

#### Formation factor and Archie's law

The formation factor (F) of a layer is defined by the equation

$$F = R_i / R_w \quad (4)$$

where  $R_i$  is the bulk resistivity of the layer and  $R_w$  is the resistivity of the saturating groundwater. After considering problems of nonuniqueness, a value for bulk resistivity is obtained from the model of a VES curve performed near a borehole while a value for groundwater resistivity is obtained from water in the borehole. A groundwater sample that is presumably representative of the groundwater that saturates the layer is bailed or pumped from the borehole. The specific conductance of the water sample is measured along with the temperature as soon as the

water reaches the surface. Specific conductance and conductivity are interchangeable terms and both are equivalent to the inverse of resistivity. Since specific conductance (SC) is the common measure of the electrolytic conductivity of a solution and is measured in micromhos / cm by most instruments, it can also be expressed as a resistivity in ohm-feet by the equation

$$R_w \text{ (ohm-ft)} = 32,800 / SC \text{ (micromhos/cm)} . \quad (5)$$

The specific conductance of an extracted water sample will closely approximate the true conductivity of the water in the aquifer if the water is highly mineralized (Keller and Frischknecht, 1966). Thus, for a polluted layer with a consistent rock matrix and void space geometry, the formation factor remains constant even if the degree of pollution changes the groundwater resistivity and the bulk resistivity. An exception to this statement is where the groundwater becomes relatively uncontaminated and dilute. In such cases the groundwater resistivity calculated from the specific conductance measurement of an extracted sample may be higher than the true groundwater resistivity. This is due to the in situ effects of two phenomena: surface conductance and ionization of clay minerals.

Briefly, surface conductance occurs when several layers of water molecules become adsorbed to the surfaces of silicate minerals in the rock matrix (Keller, 1967). This would cause only a slight increase in the resistivity of



highly-mineralized groundwater due to the higher viscosity at the surfaces reducing ion mobility. More important, however, is the decrease in resistivity of relatively pure groundwater by proton transfer between water molecules in the adsorbed layer. Keller comments that both of these effects are more pronounced in fine-grained rocks as is also the effect of ionization of clay minerals. This phenomenon occurs when exchangeable ions are desorbed from clay minerals in the rock matrix in a process resembling ionization. The resistivity of the groundwater is decreased by the higher concentration of ions available for electrolytic conduction. Once again, surface conductance and ionization of clay minerals only present a problem in the measurement of specific conductance in an extracted dilute groundwater sample.

Once a formation factor is derived for a layer, it can be used to calculate groundwater resistivities, and thus specific conductances, at other VES sites from their modeled layer resistivities. At this point a qualitative assessment of the degree of pollution can be made at each VES center point. The assessment can be made more quantitative if a specific conductance value for unpolluted natural groundwater in the area is known. By knowing the temperature of the groundwater when the specific conductance measurement was made, the approximate salinity of the groundwater at each VES location can be obtained from published nomograms (Keys and MacCary, 1971).

As was previously stated, there is a dependence of bulk resistivity in a saturated layer not only on the resistivity of the groundwater in the void spaces, but on the volume and distribution of the void spaces themselves. This dependence is expressed in the following empirical formula known as Archie's law (Archie, 1942):

$$F = R_i / R_w = A n^{-m} \quad (6)$$

where  $n$  is the total porosity (decimal form) of a layer. The value of  $m$  is a function of the void space geometry and is sometimes referred to as the cementation factor. It is determined by making a number of measurements on the same material of known porosity saturated with water of different resistivity. Ordinarily, this is not practical and a published value for a similar material can be substituted. Sometimes the value of  $A$  in equation 6 is estimated to be unity. Archie's law was developed for the petroleum industry to relate borehole resistivity measurements to sandstone and limestone porosities of 5 to 25 percent. More recently, Archie's law has been applied to fractured media, as will be seen later.

Using the derived formation factor and Archie's law, the porosity of the layer can be determined. The porosity value ( $n$ ) is used to calculate the average linear velocity ( $v$ ) at which pollutants are flowing in the layer by the equation

$$v = (-K / n) dh/dl . \quad (7)$$

K, in this case, is known as hydraulic conductivity which is a term that embraces not only the permeability of the rock matrix, but also the properties of the polluted groundwater (Freeze and Cherry, 1979). The ratio  $dh/dl$  is called the hydraulic gradient and can be derived from measurement of the static water level elevations in three or more boreholes.

#### AB Rectangles

The AB rectangle method is a refined version of horizontal profiling in that a map of the areal variations of apparent resistivity can be produced. Although the method is described by Kunetz (1966) and mentioned by Zohdy et al (1974), its use is not widespread. It is included here because it is a potentially valuable technique for the detailed investigation of conductive pollution in fractured rock.

Unlike horizontal profiling, the AB rectangle method is performed using the Schlumberger array. Unlike a VES, the potential electrodes do not always remain colinear with or centered between the current electrodes. Instead, the current electrodes, A and B, are kept stationary while the

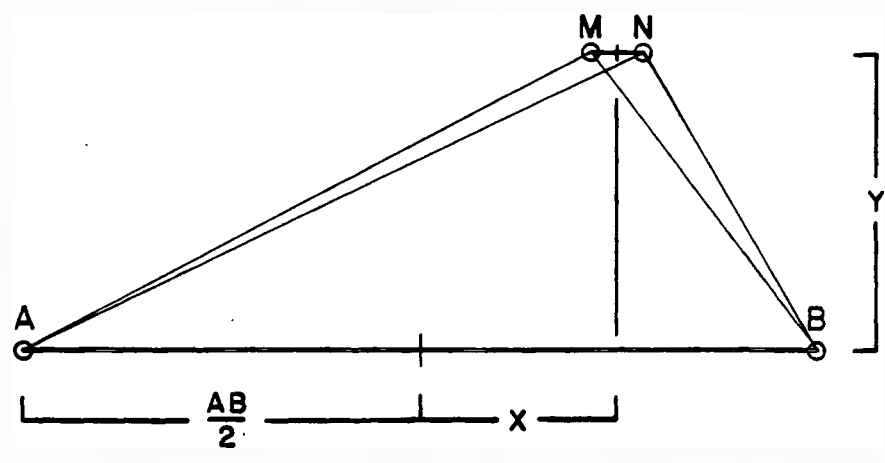
potential electrodes, M and N, are moved about the center point of the array in a grid pattern. The potential electrodes are kept in the middle third of the distance from A to B and within a lateral distance of  $AB/4$  on either side of the line AB, hence a rectangle. The separation between M and N is held constant and their orientation is kept parallel to AB.

When calculating apparent resistivities, the geometric factor, K, must be calculated separately for each position of MN. K is derived by using the geometry and equations described in figure 5a and the general equation

$$K = 6.28 / [ (1/AM) - (1/BM) - (1/AN) + (1/BN) ] \quad (8)$$

A short program that will calculate the K value for any values of  $AB/2$ , MN, X, and Y was developed during the present investigation. The program is included in Appendix A.

As with horizontal profiling, it is necessary to perform a VES, preferably where the center point of the AB rectangle will be. The resulting field curve is evaluated to determine what  $AB/2$  values will cause an optimum contribution by the desired layer. Several  $AB/2$  values are chosen so that apparent resistivity variations for more than one depth can be mapped. The approximate depth of investigation for each AB rectangle map is estimated from a geoelectrical model of the VES curve. It should be noted that the depth of investigation varies slightly within the



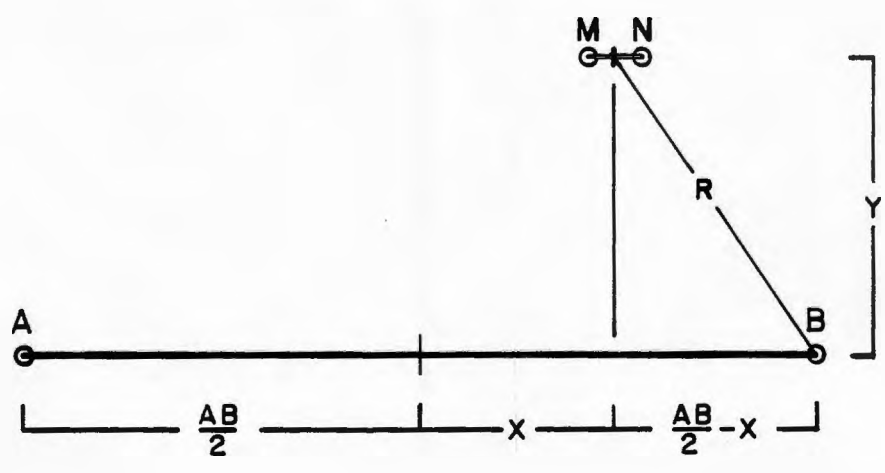
$$AM = \sqrt{\left(\frac{AB}{2} + X - \frac{MN}{2}\right)^2 + Y^2}$$

$$AN = \sqrt{\left(\frac{AB}{2} + X + \frac{MN}{2}\right)^2 + Y^2}$$

$$BM = \sqrt{\left(\frac{AB}{2} - X + \frac{MN}{2}\right)^2 + Y^2}$$

$$BN = \sqrt{\left(\frac{AB}{2} - X - \frac{MN}{2}\right)^2 + Y^2}$$

a. Calculation of variables in Equation 8



$$R = \sqrt{\left(\frac{AB}{2} - X\right)^2 + Y^2}$$

b. Calculation of AB/2 value (R) for computer model

Figure 5. AB Rectangle calculations

AB rectangle; it is least at the center and greatest at the edges away from the line AB. However, the influence of lateral inhomogeneities that affect the depth determination in horizontal profiling is more subdued in the AB rectangle method because of the smaller area in which measurements are taken.

Once the observed apparent resistivity distribution is obtained for each depth being mapped, the variation in the expected apparent resistivities inherent in the AB rectangle method must be derived. The geoelectric model for the interpreted VES curve is entered into the computer program for calculating theoretical curves. The distance between the MN center point and the closest current electrode (R in figure 5b) is entered as an  $AB/2$  value into the program. The program is then instructed to calculate the corresponding apparent resistivity value that occurs on the theoretical curve. Assuming that the subsurface layering is nearly horizontal and the geoelectric model is accurate, the resistivity values calculated in this way for each MN location constitute the expected apparent resistivity distribution.

For the purpose of investigating groundwater pollution, the disparity between the observed apparent resistivity distribution and the expected apparent resistivity distribution is of greatest importance. One way to analyze the disparity is to simply subtract the expected value from the observed value at each MN position. The resulting

difference can be termed a residual apparent resistivity. The residual values can then be normalized by subtracting from each the residual apparent resistivity value at the center point of the AB rectangle. This arbitrarily assigns the center point a value of zero in order to standardize all the maps at different depths. At this point, contours of equal values can be drawn easily. Areas of low or negative values, therefore, represent areas of lower-than-expected apparent resistivity which can be interpreted accordingly. It will be seen later how it may be possible to trace fractures in bedrock using this technique.

The development of the AB rectangle method has been hindered in the past by the number of time-consuming calculations that had to be made by hand. However, with the recent accessibility of calculators and computers, this method may in the near future be recognized as a feasible method for detailed resistivity mapping especially of polluted subsurfaces. With further research an automatic interpretive computer program could be developed to facilitate its use.

## HYDROGEOLOGY OF FRACTURED CRYSTALLINE BEDROCK

### Crystalline Bedrock as an Aquifer

The igneous and metamorphic rocks that comprise crystalline bedrock are considered to be impermeable in the context of many groundwater problems. In such cases the overlying aquifers of consolidated and unconsolidated sediments possess hydraulic properties that are many times greater than those of the crystalline bedrock (Freeze and Cherry, 1979). Therefore, when compared to sedimentary aquifers, bedrock is relatively impermeable. However, by virtue of the fractures it may contain, crystalline bedrock can have important hydraulic properties of its own.

To be considered an aquifer, crystalline bedrock must be able to transmit water and bear it in usable quantities. This condition is generally satisfied when fractures in the rock intersect each other to form a network of channels through which water can flow. Since most of the bedrock in New England is crystalline and not sedimentary, references to the bedrock aquifer usually imply a fractured crystalline bedrock aquifer.

Fractured crystalline bedrock aquifers differ from fractured sedimentary bedrock aquifers in that the host rock itself is relatively non-porous. A fractured-sandstone aquifer, for example, behaves differently hydrologically



than a fractured-granite aquifer. The rock between the fractures in a granite aquifer is practically solid while a moderately cemented sandstone matrix may contain at least as much water as the fractures. It will be shown later that some crystalline rocks such as schists and slates can have an appreciable intergranular porosity. Thus, even apparently solid crystalline rock can be considered somewhat porous. In general, however, crystalline bedrock is considered to be a fractured non-porous medium.

#### Fracture Types and Their Relation to Groundwater

Fractures ranging from visible to microscopic occur in nearly all crystalline rocks (Spencer, 1977). They are planar to curvilinear surfaces along which the rock has lost cohesion. A visible (large-scale) fracture where there has been no displacement other than the movement normal to the fracture surface which causes the crack is termed a joint. Where the loss of cohesion results in the lateral, vertical, or oblique displacement of the fracture surfaces, a fault is produced. Joints and faults often occur as sets of subparallel fractures and may extend for large distances. Frequently more than one joint set is apparent in a particular crystalline rock. This leads to the fortunate inevitability that the fractures will intersect, thus increasing the rock's effectiveness as a conductor of

groundwater. Faults, meanwhile, generally occur as a zone of faults and fractures which contains much broken rock. The development of joints and faults is associated with the creation and relief of tectonic stresses in the earth.

Sheeting is a type of fracture that most often occurs in shallow igneous intrusive bodies such as granite plutons. These large-scale fractures are generally parallel to the topography and conform to the shape of the top of the pluton (Spencer, 1977). It is thought that sheeting results from the release of pressure caused by erosion of the overburden. Sheeting fractures are effective in the lateral transport of groundwater.

Horizontal sheeting fractures are closely spaced near the surface, but become more widely spaced at depth. They are probably nonexistent several hundred feet below the surface (Davis and De Wiest, 1966). The more-vertical joints are reported by Cushman et al (1953) to be spaced usually 5 to 10 feet apart, but joint spacings may vary from less than an inch to several hundred feet. Their number decreases with depth owing to increased pressures which tend to close fractures. Some faults or fault zones are assumed to extend to the focii of earthquakes several miles beneath the surface. However, most faults probably terminate before such depths are reached. It can be concluded that most large-scale fractures occur within the upper 300 feet of the subsurface.

Many of the microscopic fractures are simply cracks

between mineral grains in igneous and metamorphic rocks. In plutonic rocks small-scale cracks can form along compositional layers or flow structures as a result of the contraction of the magma as it cools. Slaty cleavage and schistosity occur in metamorphic rocks when platy minerals such as mica and ellipsoidal grains of quartz and feldspar are aligned nearly parallel during recrystallization. Schistosity generally involves larger mineral grains than slaty cleavage. Small-scale cracks in metamorphic rocks can also occur as a result of fracture cleavage. Fracture cleavage differs from slaty cleavage and schistosity in that the cracks are not parallel to the alignment of the grains. According to Hobbs et al (1976), fracture cleavage can be "closely spaced microfaults or fractures" indicating at least slight displacement whereas Billings (1972) refers to fracture cleavage as closely spaced joints indicating no displacement. Whatever the origin of the small-scale cracks, these fractures can contribute to the total porosity of a crystalline rock.

## Porosities of Crystalline Bedrock Aquifers

Normally, the various types of porosity in an aquifer are classified as either primary or secondary depending on their origin (Heath and Trainer, 1981). Pore spaces developed during formation of the rock constitute the primary porosity, while voids formed later as by fracturing are considered secondary porosity. Some authors (Freeze and Cherry, 1979; Fetter, 1980) try to avoid genetic definitions of primary and secondary porosities. They simply state that primary porosity is the volume of the void spaces within the (sedimentary) rock matrix and secondary porosity is the volume of the fractures. Confusion arises, however, when crystalline rock is considered since the void spaces within the rock matrix are usually themselves a result of fracturing. Therefore, when referring to types of porosity in crystalline rock, it seems appropriate to adopt the terms intergranular porosity for the rock matrix voids and joint porosity for the other fractures after Keller and Frischknecht (1966).

Keller and Frischknecht give normal ranges of the two kinds of porosity found in crystalline rock. They list the intergranular porosity of low-rank metamorphics as 1-8 percent of the total volume of the rock and 0-10 percent for Paleozoic and younger igneous rocks. Joint porosity ranges from 0-2 percent for both rock types. Cushman et al (1953) add that most crystalline rock in New England contains less

than 1 percent total porosity.

The width of fractures in crystalline rock affects the volume of water that can be stored and potentially transported. Fractures are generally less than  $1/25$  inch (1mm) wide (Freeze and Cherry, 1979) though they may certainly have a greater width (Davis, 1969). The width of the fractures that comprise intergranular porosity may be miniscule. Thus from the viewpoint of well yields, the volume of water derived from intergranular porosity is insignificant compared to the volume of water obtained by joint porosity. However, from the viewpoint of the electrical resistivity of saturated crystalline rock, the water within the intergranular pore structures can be of greater significance, as will be seen later.

Another factor that affects the porosity (and the resistivity) of fractured crystalline rock is the geological phenomenon of weathering. Of the two types of weathering, chemical and mechanical, chemical weathering is primarily responsible for the enlargement of fractures in buried bedrock. It results in the decomposition of certain minerals that may be exposed along the fracture surfaces. Elements of a mineral may be leached and carried away in solution by the groundwater. Davis (1969) gives a hypothetical example of a pure quartz rock yielding dissolved silica causing the increased width of a fracture over a long period of time. The extent to which the fracture width increases is determined in part by the

residence time of groundwater in the fractures. If the residence time is long, the groundwater will approach saturation with the leached element and the widening process will be slowed.

Elements are put into solution by another process of chemical weathering called hydrolysis. Exposure to groundwater can hydrate a mineral. Molecules of water are exchanged with elements in the mineral which are in turn put into solution and carried away by the groundwater. As a result, the composition and structure is modified and a new mineral is formed. An example is when a feldspar such as orthoclase is altered to a clay mineral such as kaolinite. Besides adding dissolved elements which slow the leaching process of fracture widening, fracture widths can be decreased by the expanded structures of the clays as a result of hydrolysis (Zumberge and Nelson, 1976).

Also counteracting the widening of fractures and the creation of new fractures by leaching is the coating of fracture surfaces with insoluble metallic oxides. These tend to clog the smaller fractures (Davis, 1969) and insulate the minerals from further leaching. Such stains can be seen on fracture surfaces in bedrock cores from water wells.

Mechanical weathering does not occur at present in bedrock at depth. Certainly, fractures in bedrock outcrops currently exposed to the atmosphere at the surface are enlarged by mechanisms such as root growth and freeze-thaw

action. Mechanical weathering may, however, have occurred in bedrock that is now buried by glacial drift during the time when the continental glacier or glaciers that covered New England existed. The extent of mechanical weathering in the bedrock of Southern New England during the Pleistocene is disputed (Feininger, 1971) and will be discussed further in the section on the geology of the Little Compton site.

#### Pollutant Flow in Crystalline Bedrock Aquifers

Most of the flow of groundwater in a crystalline bedrock aquifer occurs in the interconnected joint fractures. Although the intergranular fractures may contain groundwater, it is essentially static due in part to the force of atomic fields at the fracture surfaces (Davis, 1969). The result is that the flow of groundwater through the fractures in a crystalline bedrock aquifer is on a larger scale than, for example, is the flow of groundwater through a well-sorted, quartz-sand aquifer. This suggests that if the established principles of groundwater flow in a granular medium are to be applied to a fractured medium, a much larger volume of the fractured medium must be considered (Freeze and Cherry, 1979). As long as the fracture spacing is sufficiently dense within this volume, the blocks of material between the fractures, which at this enlarged scale are relatively solid, are proportional to the

grains of sand in the granular medium.

Benedini (1976) refers to the enlarged scale as the scale of homogeneity; a fractured bedrock aquifer, therefore, has a larger scale of homogeneity than a sedimentary surficial aquifer. This concept is useful since the empirical (Darcy) flow equations were derived from flow through a representative volume of granular material that was large enough to be considered homogeneous, instead of through the individual pore spaces which are not homogeneous in size or shape. Certainly there are problems with measuring the flow of water through fractures in rock samples (Witherspoon, 1981). Therefore, rather than having to consider the flow through individual fractures in a crystalline bedrock aquifer, the flow equations for granular materials can be transferred to the bulk flow of groundwater through a representative volume of bedrock at an appropriate scale of homogeneity. The only pitfall in transferring these equations to bedrock is the possibility of nonlinear-laminar flow or turbulent flow through exceptionally wide fractures, in which cases the Darcian flow equations would be invalid (Freeze and Cherry, 1979).

In an earlier section, equation 7 was presented to calculate the average linear velocity of pollutants flowing through fractured bedrock. This is an example of a flow equation that is valid for both granular media and fractured media assuming a sufficient scale of homogeneity for each. By analyzing this equation, it should be noted that the



inverse relationship between porosity and average linear velocity can result in significantly higher velocities in low porosity bedrock aquifers than in higher porosity surficial aquifers. Hence, as was pointed out in the introduction, bedrock pollution can be more of a threat to wells remote from a pollution source than surficial pollution. The process by which pollutants are transported by the bulk flow of groundwater is known as advection. Thus, the rate of the advection process is equivalent to the average linear velocity of the groundwater.

When considered at their respective scales of homogeneity, the paths of groundwater flow through representative volumes of a sand aquifer and a fractured bedrock aquifer are probably equally tortuous. However, when both aquifers are compared to each other at an intermediate scale, the paths in a sand aquifer will appear much more tortuous than the relatively direct fracture paths of a bedrock aquifer. It is easy to visualize in this way how advection can cause pollutants to travel farther at the same average linear velocity through a fractured medium than through a granular medium over the same time period.

Hydrodynamic dispersion tends to dilute the concentration of pollutants as well as to retard the advection of pollutants through a fracture network (Freeze and Cherry, 1979). Two processes of hydrodynamic dispersion are important in fractured rock: mechanical dispersion and molecular diffusion. Both of these processes operate on a

microscopic scale, although the effects of mechanical dispersion are more macroscopic. Mechanical dispersion is the spreading out of pollutants both in the direction of groundwater flow (longitudinal dispersion) and perpendicular to it (transverse dispersion). Longitudinal dispersion is usually stronger than transverse dispersion explaining why pollution plumes are often elongate. Mechanical dispersion in shallow bedrock results from drag exerted on the groundwater by irregularities on the fracture surfaces and by variations in fracture width along the flow path. This causes the velocity of groundwater at the center of fractures to be higher than at the surfaces. Molecular diffusion occurs in areas of the aquifer having low velocity such as in the intergranular pores of the rock matrix. By their own potential to move to a less concentrated area, ions in polluted groundwater will penetrate the intergranular pores until equilibrium is reached. It is important to note this process for the later consideration of electrical conductance and resistance in the rock matrix.

While mechanical dispersion alone can be responsible for the shape of a volume of polluted groundwater in both granular and fractured aquifers, anisotropy with respect to fluid flow expressed by fractured bedrock aquifers will most often determine the extent of pollution in such aquifers. Anisotropy occurs when hydraulic conductivity ( $K$  in equation 7) is not constant for all directions. Obviously, in a small volume of rock containing a fracture, the hydraulic

conductivity is greatest along the plane of the fracture. When considered at the rock's scale of homogeneity, anisotropy disappears if all the fractures are randomly oriented. However, as is usually the case, fractures in bedrock are oriented according to the stress that formed them. Even though several alignments of fractures may be present in a bedrock aquifer, there still may be a preferred direction of pollution transport independent of the hydraulic gradient and the effect of mechanical dispersion.

#### Geology and Hydrogeology at Little Compton, R.I.

The subsurface in the vicinity of the Little Compton State Garage is composed of two geologic formations: glacial drift overlying crystalline bedrock. The glacial drift consists entirely of till which forms an unconsolidated surficial aquifer. The crystalline bedrock is most likely mica-chlorite schist which is fractured in several directions rendering it an aquifer. Approximately 80% of the water supply in the Tiverton - Little Compton, R.I. area is from individual wells of which 6 out of 10 are completed in bedrock (Schiner and Gonthier, 1965). The bedrock aquifer is reportedly the more reliable source of groundwater although yields are rarely sufficient for more than domestic supplies.

The site of investigation at Little Compton includes

the State Garage property and the properties immediately to the north and to the south (see figure 1). This area is estimated to be 6 acres (2.4 hectares). The site occupies the nearly-level, central portion of a topographic saddle at an elevation of approximately 80ft (24.4m) above mean sea level. Subsequently, there are only slight slopes towards the swamp to the east and a drainage ditch along Willow Avenue to the west. At one time surface runoff flowed towards the yard of the house south of the State Garage, but it has since been diverted. The groundwater supply of this house is from a dug well in the surficial aquifer and is contaminated beyond potability. The resident of the house must get his drinking water from the State Garage's deep bedrock well which is as yet uncontaminated. The residents of the house north of the State Garage also receive their water from an uncontaminated deep bedrock well.

The road deicing salt is kept covered in a storage shed that is open on one side. The sand-salt pile is stored uncovered on asphalt pavement during the winter and spring and thus is exposed to precipitation. An underground tank has been installed to collect polluted runoff towards Willow Avenue but was frequently seen to have overflowed during heavy rains. Runoff towards the swamp flows uncontrolled.

According to notations made during the drilling of the two shallow bedrock wells at the State Garage site, approximately 15ft (4.6m) of compact, silty gray till was encountered before bedrock was reached (Urish, 1980). It

would be expected that a poorly-sorted, fine-grained material such as this would retard the infiltration of polluted water and contain it. An average linear velocity of less than one inch (several millimeters) per year is not unreasonable for a silty till. The fact, however, that high concentrations of salt have penetrated well into the fractured bedrock indicates that the till itself may contain fractures. Field measurements of bulk hydraulic conductivity in jointed till are reported to be 1 to 3 orders of magnitude larger than laboratory measurements of unfractured till matrix (Freeze and Cherry, 1979). The effect of joints in an unsaturated surficial deposit of till is to increase the rate of infiltration of polluted runoff. The effect of joints in the saturated zone is to increase the rate of recharge to the bedrock aquifer (Williams and Farvolden, 1969). An alternate explanation may be that osmotic pressures have allowed the high salinity groundwater to penetrate the till.

The only outcrops of bedrock in the vicinity of the Little Compton site are to the north and west (figure 6), the closest being more than 1/2 mile (0.8km) away. A lone outcrop of granite occurs 1 mile (1.6km) north of the site and is a part of the Bulgarmarsh Granite (Pollock, 1964). At this outcrop the granite is gray, coarse-grained, weakly foliated and jointed. The foliation and joints strike northeast. Pollock suggests that the foliation represents original flow structures since in many places it parallels

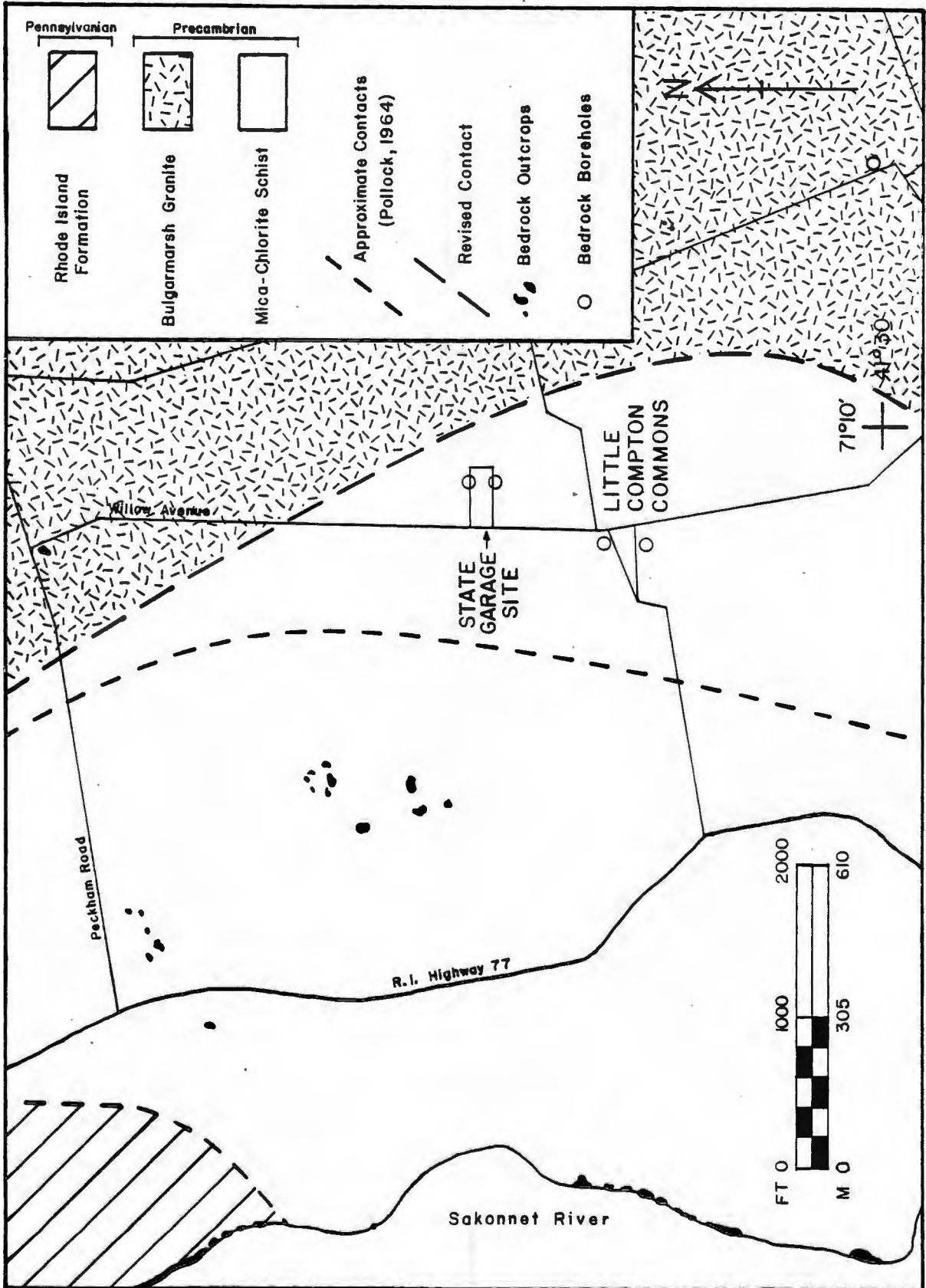


Figure 6. Bedrock geology at Little Compton

the schistosity of the overlying mica-chlorite schist host-rock. The other outcrops in the vicinity, including the one closest to the site, are of mica-chlorite schist. The texture of the gray to green schist is fine-grained to almost phyllitic at the outcrops east of Main Road. Thin bedding, which the schistosity parallels, is highly contorted and sheared at some outcrops likely indicating proximity to the granite contact. Away from the granite, the bedding and schistosity are even and both strike northeast. Thin beds of limestone are observable in many of the mica-chlorite schist outcrops. Additionally, two sets of fracture cleavages trending northeast can be distinguished on the outcrops.

The most recent bedrock geologic map of the Tiverton 7 1/2-minute Quadrangle (Pollock, 1964) indicates the Little Compton site is located on top of Bulgarmarsh Granite. However, the bedrock encountered in the two bedrock boreholes on the site (Urish, 1980) and in two additional boreholes in the Commons less than 2000ft (610m) south of the site (U.S. Geological Survey, 1963) is described in well reports as being "soft gray rock" or "slate". Since it is unlikely that Bulgarmarsh Granite could be misidentified as "soft" or "slate", the bedrock beneath the State Garage is probably mica-chlorite schist. From the outcrop and borehole data previously mentioned in addition to the indication of granite in a borehole southeast of the site, a revised approximate contact between the rock units is

presented in figure 6.

The type of bedrock is consequential hydrologically since the schist is potentially more permeable than the granite. Besides the intergranular porosity added by schistosity and fracture cleavage, the shearing fractures of the schist increase joint porosity over that found in the granite. Quartz veins in the granite outcrop and in the boreholes indicate the State Garage is near the schist-granite contact and that granite probably exists at some depth beneath the schist at the site. Pollock (1964) has recognized the presence of a transition zone near the contact at some outcrops within the quadrangle.

A brief conjectural geologic history of the area will further describe the geology and hydrogeology of the Little Compton site. During the Precambrian, the thin beds of volcanic and marine sediments in the mica-chlorite schist were deposited and became deeply buried. At some time before the intrusion of the Bulgarmarsh Granite the sediments underwent low-grade regional metamorphism to the upper greenschist facies. The schist formation has been correlated with similar units of the Blackstone Series in other parts of Rhode Island and Connecticut. The mica-chlorite schist was folded and fractured by intrusion of the Bulgarmarsh Granite during the Late Precambrian Avalonian orogeny. Recent radiometric age dates show that the granite crystallized 600-650 million years B.P. (Zartman and Naylor, in press). Contact metamorphism of the



schist increased its metamorphic rank to the albite - epidote - amphibolite facies in the vicinity of the site. During the Pennsylvanian period, the conglomerates, sandstones, and shales of the Rhode Island Formation were deposited in the Narragansett Basin. This formation unconformably overlies the schist and the granite; its southeastern limit is within 2 miles (3.2km) of the Little Compton site. The Rhode Island Formation was metamorphosed during the Alleghenian orogeny, which had a negligible effect on the pre-Pennsylvanian rocks. However, this orogeny may have formed one of the northeast trending fracture cleavages seen in the schist. The hydrologic significance of the several orogenic events which have affected the schist is the development of several fracture directions. These different orientations of fractures have resulted in an interconnected fracture network through which groundwater now flows.

For over 200 million years the schist, the granite, and the Rhode Island Formation underwent deep chemical weathering and erosion. Thoroughly decomposed rock undoubtedly covered the surface and was continuous with the reddish-brown saprolite that today covers the Piedmont of the southeastern states. A gradational zone perhaps 100ft (30m) or more thick occurred between the surface and fresh rock. Within this layer existed all proportions of decomposed rock, slightly decomposed rock, and blocks of unweathered rock.

The weathered rock layer remained undisturbed except for the possibility that glaciofluvial sediments were deposited at the surface from glaciers farther north before 20,000 years B.P. At that time a continental glacier advanced over the region. A theory expressed by Feininger (1971) suggests that the saturated weathered rock became frozen and was incorporated in to the base of the southward moving glacier. The furthest extent of glaciation in the Little Compton area is less than 20 miles (32km) away in what is now the Atlantic Ocean between Block Island and Martha's Vineyard (see figure 1). Considering the proximity of the leading edge of the glacier and the low gradient of the fresh bedrock surface, it is doubtful that the weathered material was transported far. A tremendous amount of subglacial water developed at the base of the glacier where the pressure-melting point was exceeded. The water was sufficient to flush residual clay particles from the weathered material leaving behind the silt-sized and larger particles that have since been deposited as till. The cobbles and boulders present in the till were derived from the partially solid blocks of rock that were loosened by chemical weathering. These weathered blocks containing a core of fresh rock were rounded by abrasion against each other in the glacier and in the glacial meltwater. The numerous boulders of conglomerate may have been transported in the basal debris at least the distance they are from the Rhode Island Formation or they may have been transported

along higher level, faster moving shear planes in the ice.

This theory for the origin of till in the area may be disputed by some geologists because it does not ascribe a prominent role to the mechanical weathering and subsequent erosion of unweathered fractured bedrock. However, it is conjectured that the fracture openings present today in the bedrock were open prior to the glacial advance and that the number of new fractures created by freeze-thaw action or by the release of overburden pressure is minimal. The theory presented ascribes a minor role to the grinding down of the fresh bedrock surface as a source of till, a process that would tend to diminish the number of fractures in the bedrock. Chemical weathering and tectonic forces therefore have played a greater role in the development of bedrock porosity at Little Compton than has mechanical weathering.

The formation of joints in the till is itself problematic. A likely mechanism for their development is the seasonal and long-term cyclical fluctuation of the water table within the till. During the 10,000 years of its existence, it is likely that the entire 15ft (4.6m) thickness of till has from time to time not been completely saturated. With the water table in the bedrock aquifer, the silty till contracts as it dries out creating tension fractures throughout the layer. Infiltration of runoff during the normal spring recharge causes the unfractured till matrix to swell but the hairline fractures remain.

## ANALYSIS OF RESISTIVITY IN CRYSTALLINE BEDROCK

### Need for Field Research

Two significant generalizations have been made thus far about crystalline bedrock, one concerning its ability to transmit an electrical current and the other concerning its ability to transmit groundwater. To recapitulate, it was stated that bedrock, including crystalline bedrock, is often interpreted to be a nonconductor of electrical current. It was also stated that in studies where bedrock is of secondary importance to the overlying sedimentary aquifers, crystalline bedrock is considered to be a "nonconductor" of groundwater. However, it was shown that if there are enough interconnected fractures present, crystalline bedrock may be an effective transmitter of groundwater. Since water is the most important component of a geoelectric layer in determining the layer's bulk resistivity (Keller, 1967), it seems reasonable to consider that there may be situations where crystalline bedrock does not behave as a nonconductor of electrical current.

If water-filled, interconnected fractures are present in a crystalline bedrock, most of the electrical current can be conducted electrolytically through the groundwater provided enough ions are present in the solution. As was stated earlier, the effect of the resistivity of the rock

matrix becomes insignificant when the electrical current flows mostly through the groundwater. In this way a layer of fractured crystalline bedrock saturated with sufficiently conductive groundwater may behave not as a nonconductor, but as a layer of finite resistivity.

Continuing this rationalization further, if a layer of fractured crystalline bedrock can have a finite resistivity that is determined by the conductivity of the saturating groundwater, variations in the groundwater conductivity due to different degrees of pollution can conceivably be detected using any of the three surface resistivity methods previously discussed. This concept is the basis for the present investigation into the applicability of resistivity methods to detecting pollution in crystalline bedrock aquifers.

Resistivity investigations are more commonly conducted in unconsolidated sedimentary aquifers than in bedrock aquifers. Subsequently, literature describing the use of resistivity for investigating bedrock is limited. Some relevant field studies include a paper by Frohlich (1973) where VES interpretations detected saline groundwater in the fractures of limestone bedrock in Missouri. Papers by Satpathy and Kanungo (1976) and Verma et al (1980) discuss how resistivity was used to find groundwater in igneous and metamorphic bedrock on the subcontinent of India. A thesis by Beissel (1971) discusses the use of resistivity to determine the orientation of buried joint sets in the

crystalline bedrock of Colorado. Another thesis by Shipman (1978) concludes that VES curves adequately detected the saltwater-freshwater interface within the sedimentary bedrock of the Narragansett Basin in Rhode Island. Few, if any publications, however, address the current topic of detecting, in crystalline bedrock, mineralized groundwater pollution that originated from a source at the surface.

#### Previous Studies on Rock Samples

While the field use of resistivity in crystalline bedrock has been limited, laboratory research of resistivity in crystalline rock-samples has been extensive. In response to the possibility that earthquakes may be predicted using resistivity, Brace et al (1965) initiated research into the change of resistivity with increasing pressure on water-saturated igneous rock samples. Although the effects of pressure on resistivity is irrelevant in shallow bedrock, a result pertinent to the present topic is that the conduction of electricity through crystalline rock with as little as one tenth of a This suggests that conduction occurs along fluid-filled microscopic cracks between mineral grains even in crystalline rocks that appear to be solid. More importantly, the same dependence of resistivity on porosity empirically observed for porous sediments was obeyed in all of their rock samples saturated with

mineralized water. In other words, Archie's law apparently also applies to crystalline rocks.

At this point it is necessary to introduce the two types of void spaces that occur at both scales of porosity. Previously, bedrock porosities were classified as being either joint porosity or intergranular porosity primarily on the basis of their relative sizes. For both types of porosity, those voids that are larger, more spherical or tubular in shape, and provide most of the storage in a bedrock aquifer are called storage pores. Those voids that are finer and flatter, and provide connection between the storage pores are called cracks or connecting pores (Keller and Frischknecht, 1966).

Brace et al. (1972) present photomicrographs of storage pores and cracks in a sample of Westerly granite from Rhode Island and a quartzite sample from Vermont as seen by using a scanning electron microscope. Nearly equant-shaped storage pores, as well as cracklike connecting pores, can be seen in abundance both within grains and along grain boundaries. The two types of void spaces often alternate along a fracture and are separated by thin bridges of uncracked material, thus being blunt-ended rather than dying out as a sharp crack. The extent as well as the connectivity of all of these pores normal to the thin sections is not known. However, results of porosity experiments imply that even pores that represent only a fraction of a percent of the rock volume are interconnected

and accessible to conducting fluids (Greenberg and Brace, 1969; Madden, 1976).

It can be concluded, then, that most of the resistance to current flow is met in the connecting pores (Keller and Frischknecht, 1966) where the fluid volume is smaller and the path of the current is longer than in the storage pores. The presence of thin bridges of material across the cracks may also tend to increase the resistance. The pore structure of a crystalline rock in two dimensions can be described as an array of polygons representing storage pores connected to each other by lines representing connecting pores. Depicting the structure of pores in this way, several authors (Greenberg and Brace, 1969; Shankland and Waff, 1974; Madden, 1976) have used networks of electrical resistors to model the conduction of electrical current through crystalline rock.

A network of resistors represents the interconnected fluid fraction of a saturated rock and thus is analogous to the porosity of the rock. The intersections of fractures in a rock are represented by the intersections of the resistor elements in the network. Since most fractures form a three-dimensional network, cubic networks of resistors are often used as models; however, two-dimensional resistor networks have been used to model two-dimensional fracture networks that have from 2 to 6 fracture planes intersecting (Greenberg and Brace, 1969). Since it appears that crack widths affect the conductivity of cracks, the resistances of



the resistor elements are varied throughout a network to simulate the wide range of crack widths in a low porosity crystalline rock (Madden, 1976). Madden's work shows that the conductivity, and thus the resistivity, of low porosity fractured rocks is controlled by the "microcrack" population even though it accounts for only a fraction of the total porosity.

The usual process during network analyses is to eliminate resistors from the array which simulates a decrease in porosity in a fractured rock. Thus, Archie's law can be tested since various values of porosity can be represented. The results of these analyses appear to confirm the earlier statement that Archie's law is adhered to even in crystalline rocks. It is also observed that Archie's law behaves for rocks with low porosities only when there is a wide range of crack widths available for current flow. Fortunately, this condition occurs in most crystalline rocks. Additionally, resistivity is relatively unaffected by the number of intersections made by fractures at any one point. Madden concludes that Archie's law is a property of the particular void space distribution within a fractured rock and not a fundamental property of the rock matrix.

It will be worthwhile to derive some resistivity values for crystalline rock from the results of these laboratory tests for comparison later with the results at Little Compton. In addition to the samples of Westerly granite

from Rhode Island that Brace et al (1965) tested, Brace and Orange (1968) present resistivity measurements on samples of chlorite schist from Chester, Vermont. The Westerly granite has a total porosity of 0.9%; 0.7% is storage porosity while 0.2% is connecting porosity. Unfortunately, no porosity values are given for the chlorite schist. However, an average grain diameter of 0.6 mm is reported which means that it is probably coarser-grained than the mica-chlorite schist at Little Compton. The lowest confining pressure at which the resistivity of both rocks were tested is 0.05 kb or approximately 50 times atmospheric pressure. The rock samples were kept saturated at a temperature of 20°C (68°F) and the pore pressure was maintained near zero.

With the above parameters constant, the measured resistivity of Westerly granite saturated with tap water was 27,880 ohm-ft (8500 ohm-m). The average resistivity of the tap water was 146 ohm-ft (45 ohm-m) yielding an apparent formation factor of 191. The resistivity of Westerly granite saturated with a NaCl solution was 1017 ohm-ft (310 ohm-m). The resistivity of the salt solution was 1.0 ohm-ft (0.3 ohm-m) yielding a true formation factor of 1017. The discrepancy between formation factors is due to surface conduction in the tap water-saturated sample. The effect of surface conduction is to reduce the value of bulk resistivity below its true value. A resistivity value for a chlorite schist sample saturated with tap water was not presented. However, the resistivity of a chlorite schist

sample saturated with a salt solution was 623 ohm-ft (190 ohm-m). The resistivity of the salt solution in this case was 0.82 ohm-ft (0.25 ohm-m) yielding a true formation factor of 760.

## FIELD RESEARCH AT LITTLE COMPTON, R.I.

### Horizontal Profiling

#### Instrumentation and measurement locations

A qualitative assessment was made during the summer of 1982 of salt pollution in the bedrock at Little Compton using the resistivity method of horizontal profiling. Soiltest, Inc. (model R-60) direct-current earth resistivity equipment was used to perform the horizontal profiles. This equipment consists of a null-type millivoltmeter and a power unit that measures the current it produces in milliamperes. Metal-stake electrodes were used at all electrode positions of the Wenner array. A vertical electrical sounding was performed using this same equipment. By observing where on the field curve the 45° line begins, two a-spacings that presumably would penetrate bedrock at all measuring points were chosen. The designated a-spacings were 50ft and 75ft (15.2m and 22.9m). Two profiling lines were run at two different a-spacings. Figure 7 gives the location of each measuring point and figure 8 gives a graph of the measured apparent resistivities plotted versus distance. The field data for both horizontal profiles is included in Appendix B.

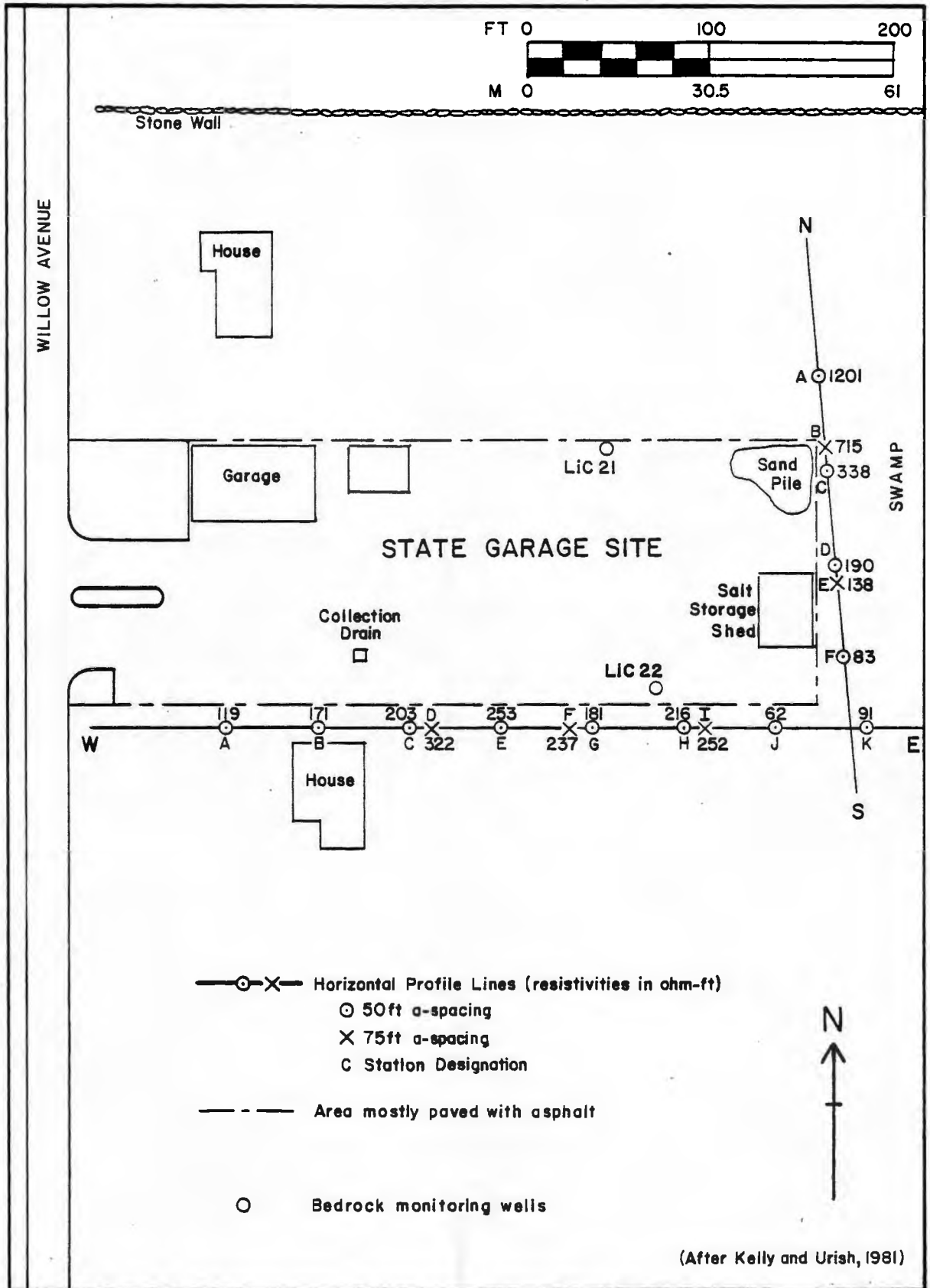
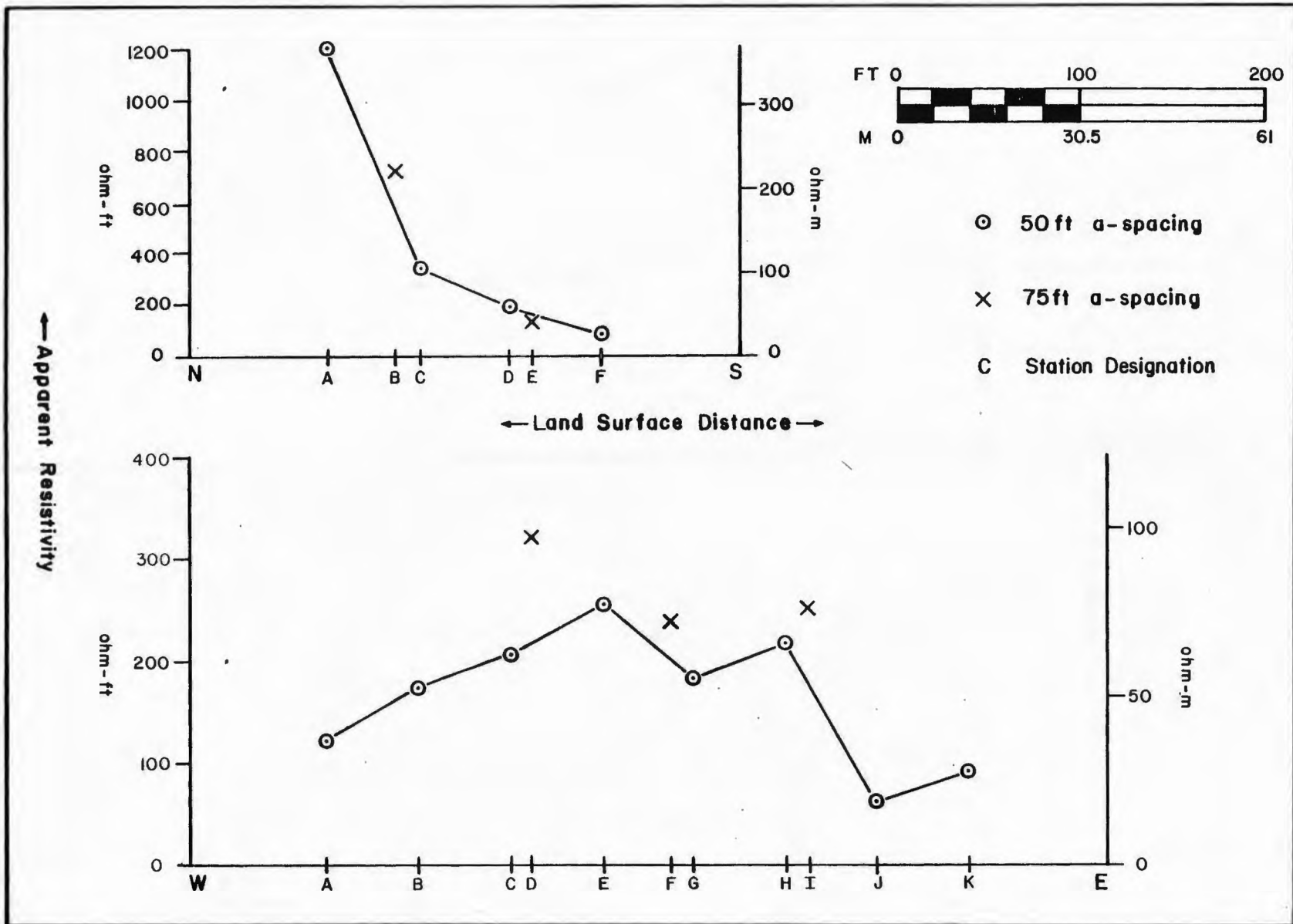


Figure 7. Location map of horizontal profiles

Figure 8. Graph of horizontal profiling resistivities versus distance



## Discussion of results

It can be seen from figures 7 and 8 that a definite apparent resistivity low occurs at the southeast corner of the State Garage property. The apparent resistivity is variable at both a-spacings on the east-west line compared to the steadily increasing values to the north on the north-south line. Intermediate lows along the east-west line can be observed near the center and near Willow Avenue. Qualitatively, it can be stated that the concentration of dissolved salt is greatest at these apparent resistivity lows and least at the northernmost measuring point. A statement, however, assigning these most-polluted areas to the bedrock aquifer would at best be cautious since the resistivity variations may be due to pollution variations in the surficial aquifer. Further consideration of the masking effect the surficial aquifer has on the bedrock will be discussed in the VES interpretations.

## Vertical Electrical Sounding

### Instrumentation and measurement locations

The Schlumberger electrode configuration was used to perform six vertical electrical soundings at the Little Compton site. Frohlich (1973) presents a schematic diagram of the equipment that was used to make each VES. A 12V car battery drives a converter which supplies current at a maximum of 0.25 amps at 400V dc. The current is regulated by several variable and constant resistors mounted on a panel and is measured by a current meter that reads milliamperes. A reversing switch on the panel allows the current flow direction to be changed. The circuit is completed with insulated wire cables connected to steel stake electrodes inserted into the ground at points A and B in the Schlumberger configuration.

The potential difference between M and N was measured with a Hewlett-Packard model 4304B dc-voltmeter. It is an analog voltmeter with a centered null reading that allows the voltage to be read in one direction and then the other when the current is reversed. The most sensitive range on the instrument is one millivolt full scale. The voltmeter was connected to two nonpolarizable porous pot electrodes positioned at points M and N in the Schlumberger configuration.



The current and the voltage were measured for both directions of current and an average was taken to cancel any spurious effects. The field data for each VES are presented in Appendix C.

Specific conductance measurements were taken in the two boreholes at the site with a Yellow Springs Instrument Co. conductivity meter. Water samples were bailed from the 6 inch (15cm) diameter bedrock wells into small containers. The conductivity electrode was placed in the water immediately after bailing. The temperature of the water sample was recorded as was the specific conductance at that temperature. These data are presented in Table 1. Also presented are water level measurements taken in the borehole before bailing was begun.

Additionally, a background water sample was obtained from the water supply of the residence north of the State Garage. A specific conductance of 408 micromhos/cm (80.4 ohm-ft or 24.5 ohm-m) at 16.5°C (62°F) was measured. Using the nomogram presented by Keys and MacCary (1971), the electrically equivalent concentration of sodium chloride approaches 250 mg/l. This is the U.S. Environmental Protection Agency's recommended concentration limit to provide acceptable potability. The lowest electrically equivalent concentration of sodium chloride derived from the borehole measurements in the polluted area is 1500 mg/l while the highest approaches 10,000 mg/l.

All six vertical electrical soundings were performed in

DATE	WELL NO.	WATER LEVEL		WATER TEMPERATURE	SPECIFIC CONDUCTANCE			
		(ft below LSD)	(ft above MSL)	(°C)	ohm-ft	ohm-m	μmhos/cm	μmhos/cm at 25 °C
3/23/83	Lic 22	1.7	79.3	9.0	3.35	1.02	9800	16,333
4/1/83	Lic 21	2.0	78.6	7.0	17.73	5.41	1850	3363
4/2/83	Lic 22	2.4	78.6	7.0	4.10	1.25	8000	14,545
4/15/83	Lic 22	—	—	10.0	3.57	1.09	9200	14,720
4/22/83	Lic 21	1.3	79.3	9.5	17.27	5.26	1900	3102
4/23/83	Lic 22	1.8	79.2	9.0	3.28	1.00	10,000	16,667

Table 1. Borehole measurements

April, 1983. VES 1 and VES 2 were made at the first of the month, VES 3 was made two weeks later, and VES 4, 5, and 6 were made one week after VES 3. A record amount of rainfall for the month of April was reported in Rhode Island causing already elevated water tables to generally rise throughout the month. Figure 9 shows the six VES center point locations in relation to the two boreholes at the site. Figures 10-15 show the field curve, the best-fit theoretical curve and the corresponding hydrogeologic / geoelectric model for VES 1-6, respectively. Note that VES 1, 4, and 5 are KH-type curves while VES 2, 3, and 6 are H-type curves.

#### Discussion of results

Because the northern well at the Little Compton site encountered bedrock at 16ft (4.9m) and the southern well encountered bedrock at 14ft (4.3m), an average depth to bedrock of 15ft (4.6m) was assumed for interpretation purposes. Depths to the zone of saturation (water table) varied with time and location between soundings and had to be interpolated from water level measurements in the bedrock wells. For the H-type curves, an initial increase in apparent resistivity typical of an unsaturated zone is not observable. Since the ground surface was extremely moist in these cases, the water table was assumed to be at the ground surface.

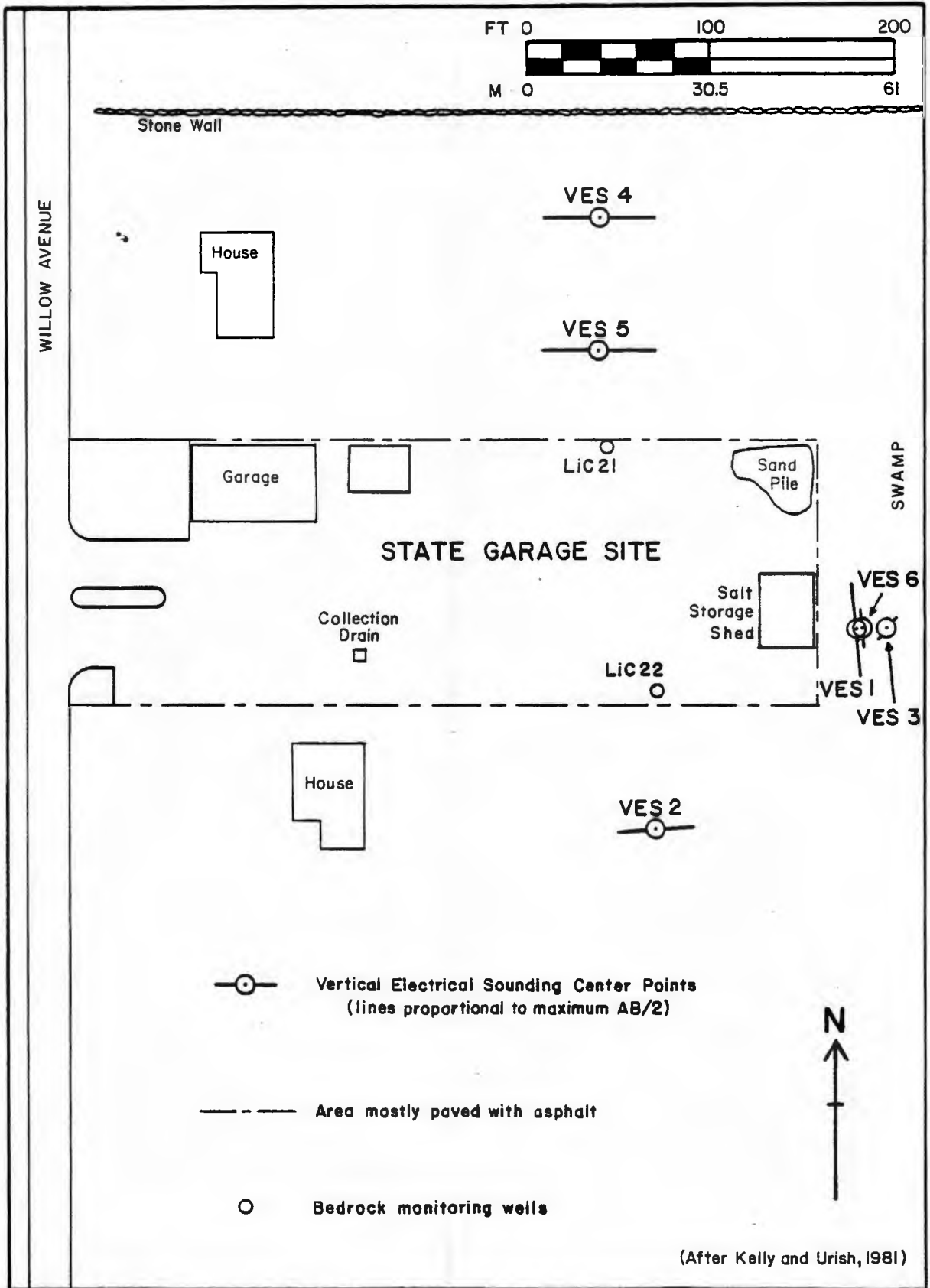
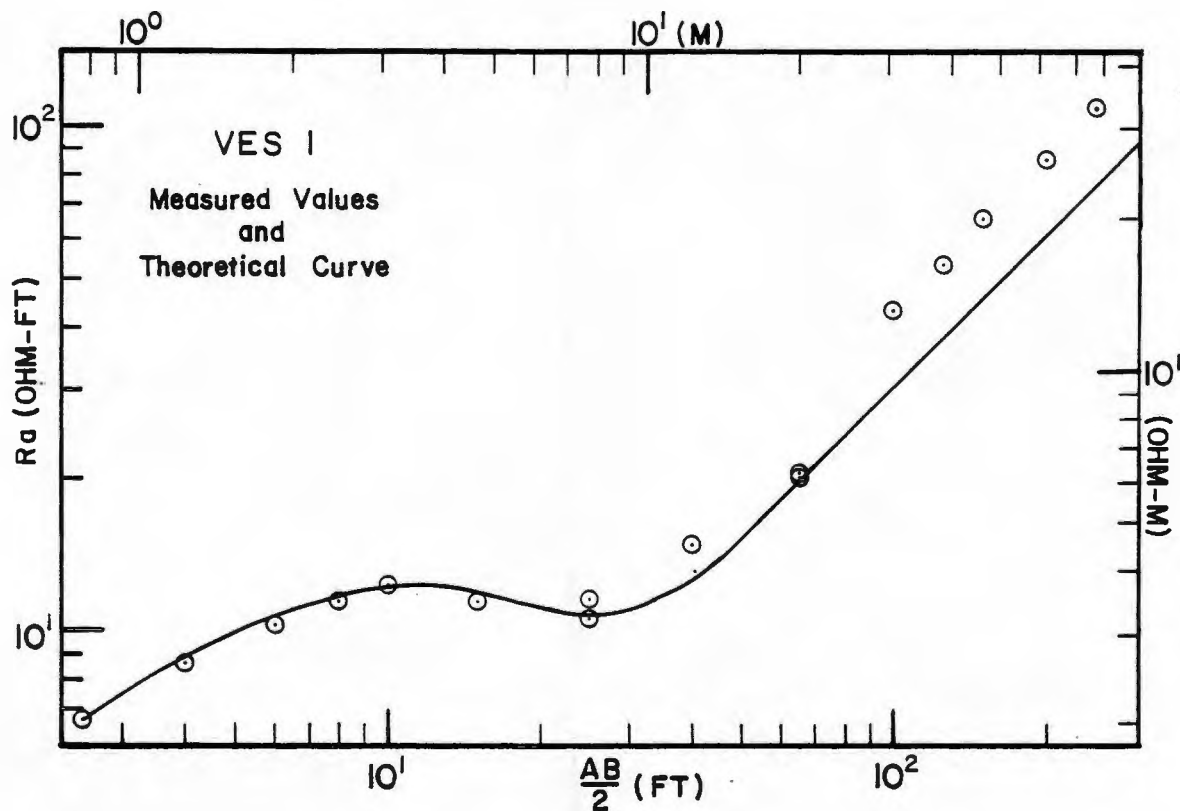
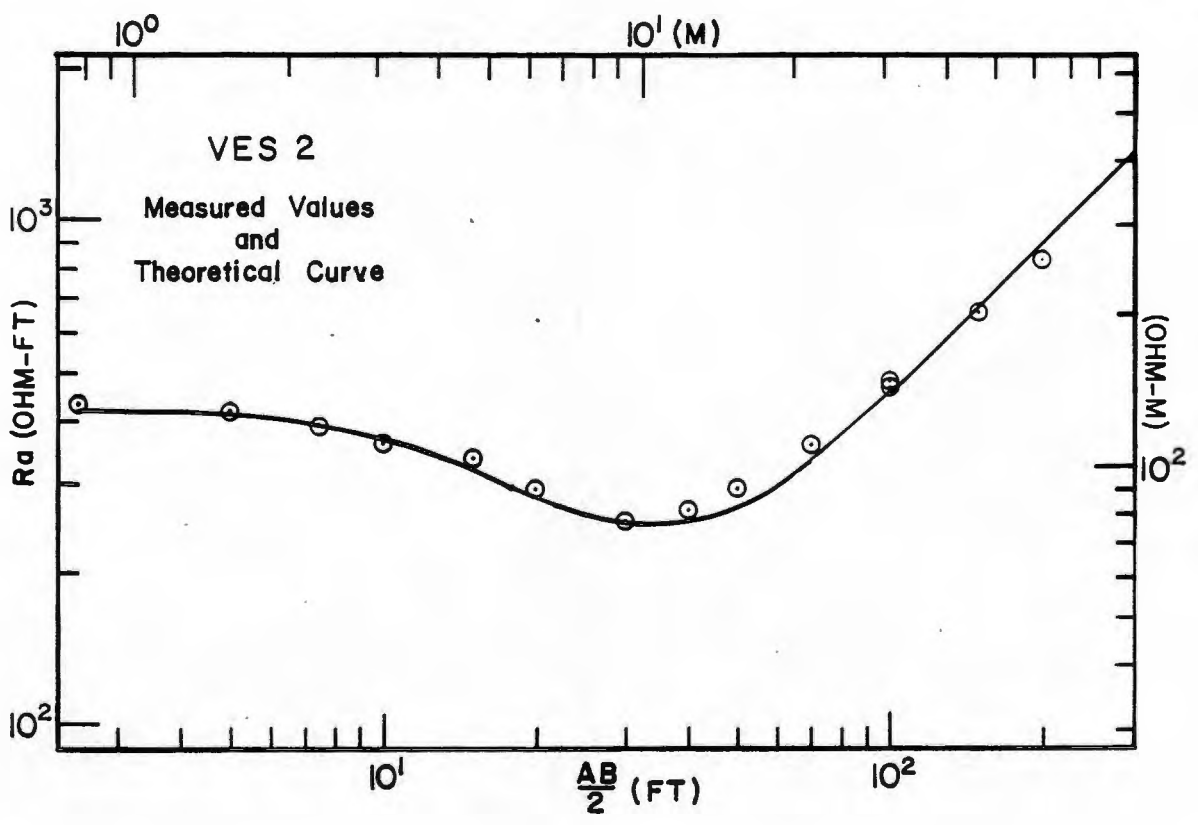


Figure 9. Location map of VES center points



DEPTH			RESISTIVITY	
(FT)	(M)		(OHM-FT)	(OHM-M)
0.7	0.2	▽ ≡	POLLUTED SOIL MOISTURE	2.6 0.8
			SATURATED POLLUTED TILL	19.5 5.9
7.0	2.1	—	MORE-POLLUTED TILL	3.0 1.0
15.0	4.6	▨	BEDROCK NONCONDUCTOR	∞

Figure 10. Field curve and geoelectric model for VES I



DEPTH		RESISTIVITY	
(FT)	(M)	(OHM-FT)	(OHM-M)
		<hr/>	
		SATURATED POLLUTED TILL	
7.0	2.1	420	128
		<hr/>	
		MORE-POLLUTED TILL AND/OR POLLUTED BEDROCK	
50.0	15.2	208	63
		<hr/>	
		BEDROCK NONCONDUCTOR	
		∞	

Figure II. Field curve and geoelectric model for VES 2

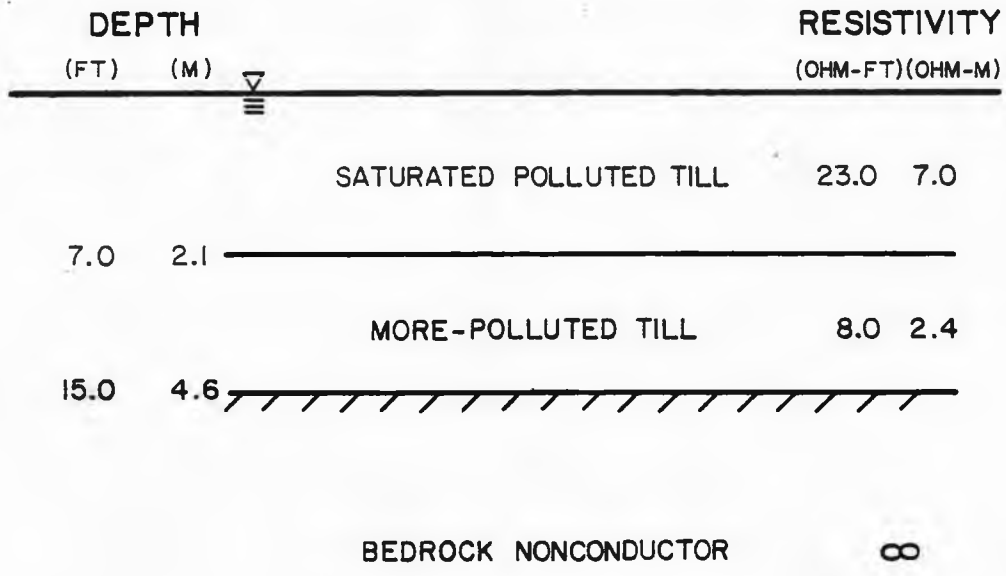
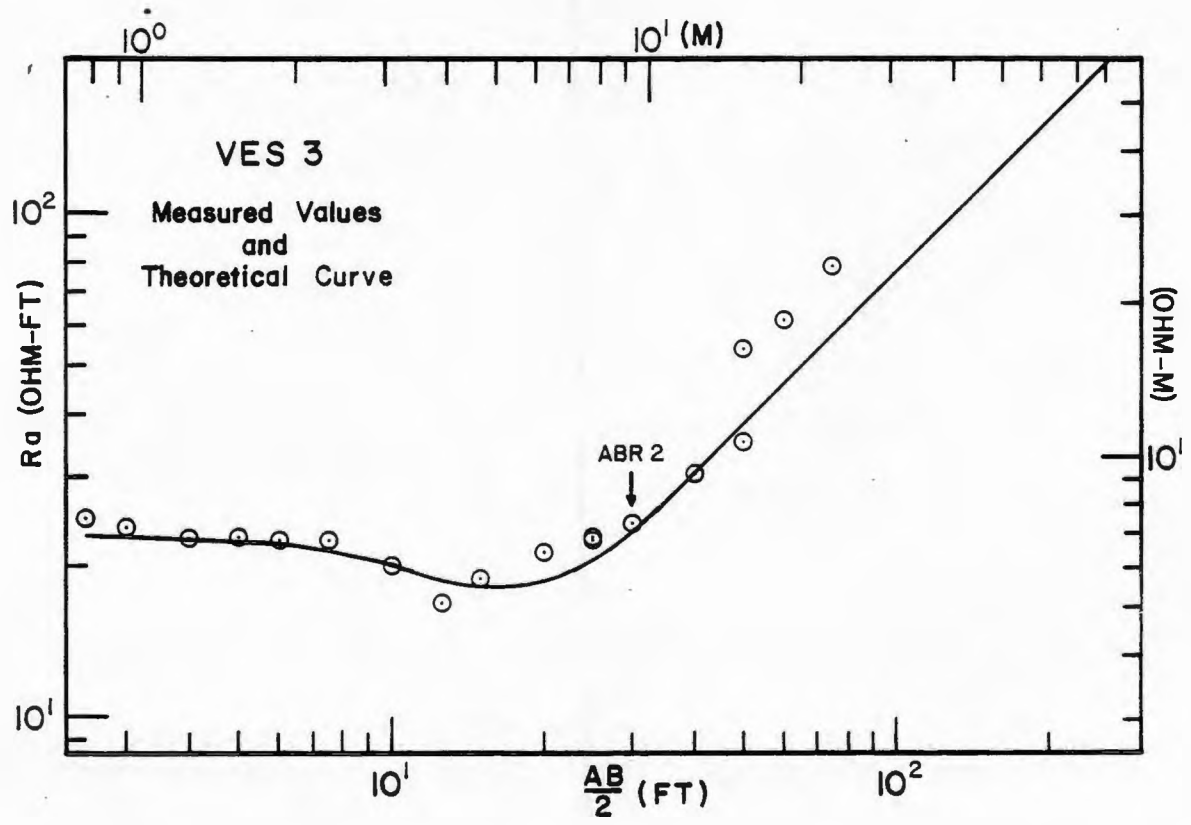
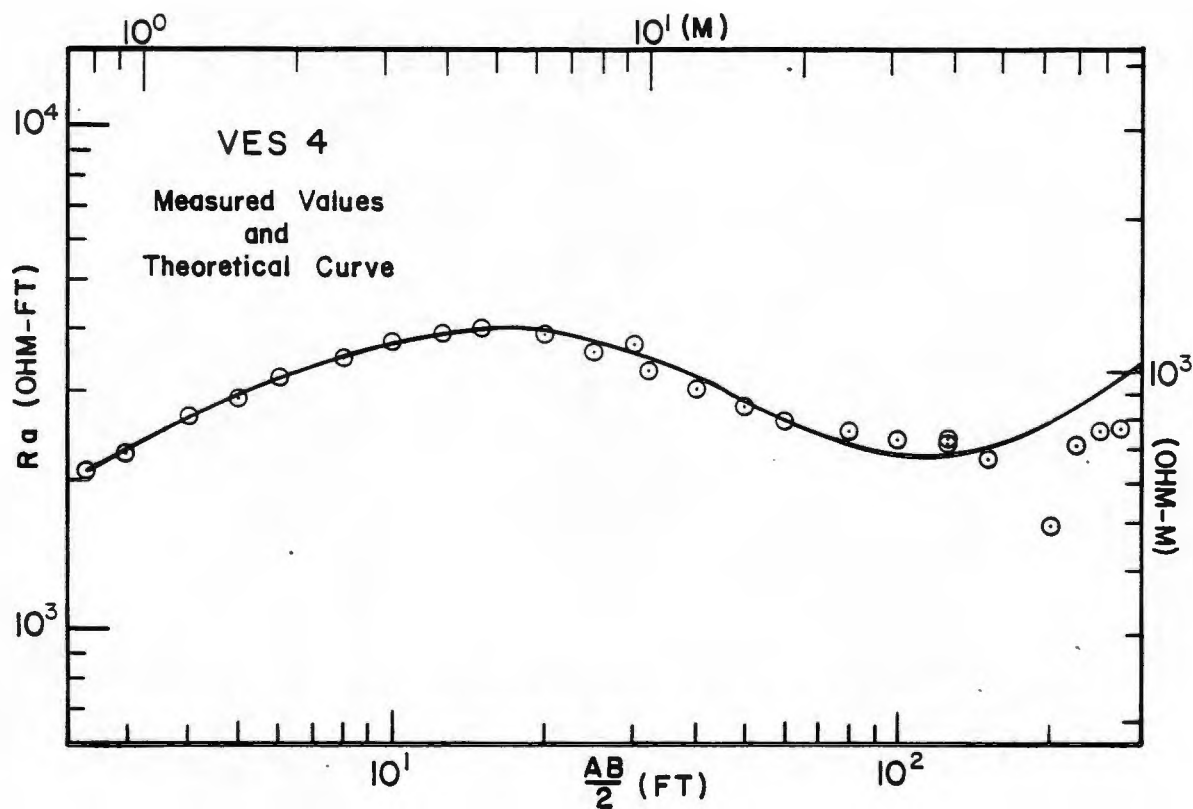


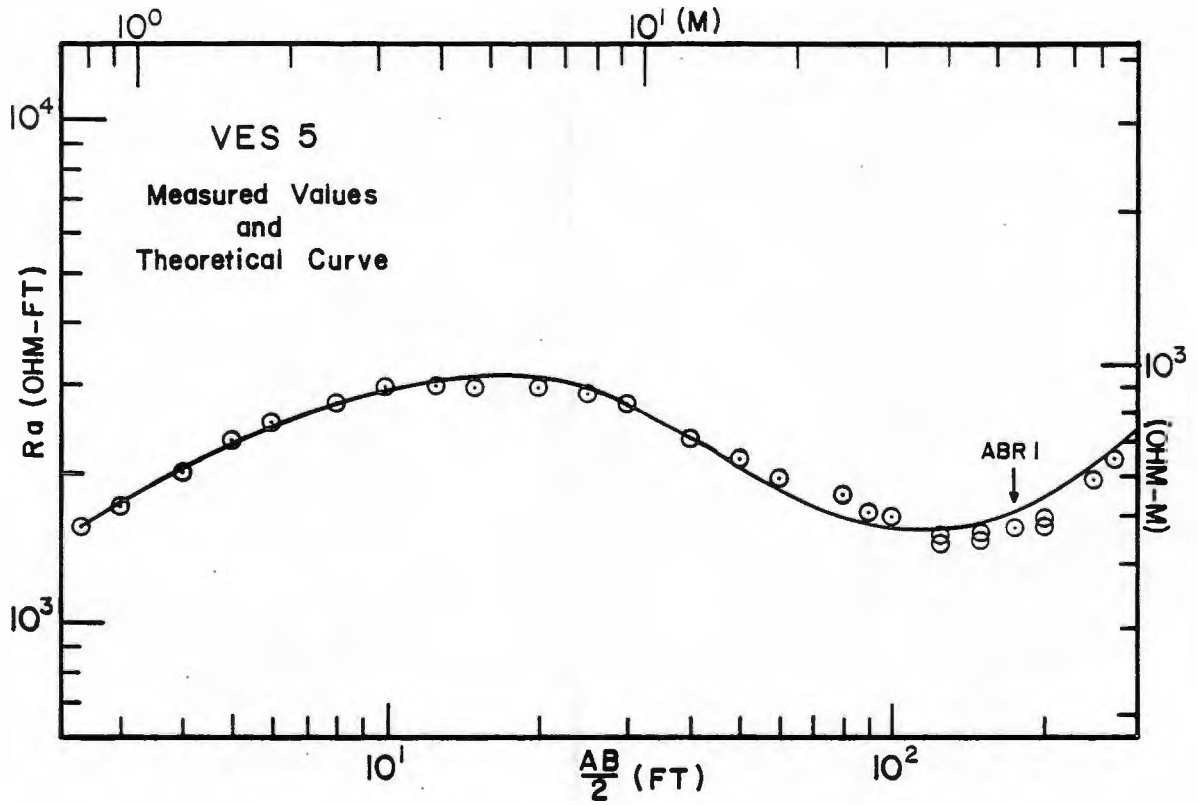
Figure 12. Field curve and geoelectric model for VES 3



DEPTH			RESISTIVITY	
(FT)	(M)		(OHM-FT)	(OHM-M)
1.3	0.4	▽ ≡	SOIL MOISTURE	1475 450
			SATURATED UNPOLLUTED TILL	4750 1448
15.0	4.6	▨	POLLUTED SCHIST BEDROCK	2000 610
192	58.5	—	BEDROCK NONCONDUCTOR	∞

Figure 13. Field curve and geoelectric model for VES 4








DEPTH			RESISTIVITY	
(FT)	(M)		(OHM-FT)	(OHM-M)
1.3	0.4	 SOIL MOISTURE	1075	328
		SATURATED UNPOLLUTED TILL	3900	1189
15.0	4.6			
		POLLUTED SCHIST BEDROCK	1325	404
175	53.3			
		BEDROCK NONCONDUCTOR	$\infty$	

Figure 14. Field curve and geoelectric model for VES 5

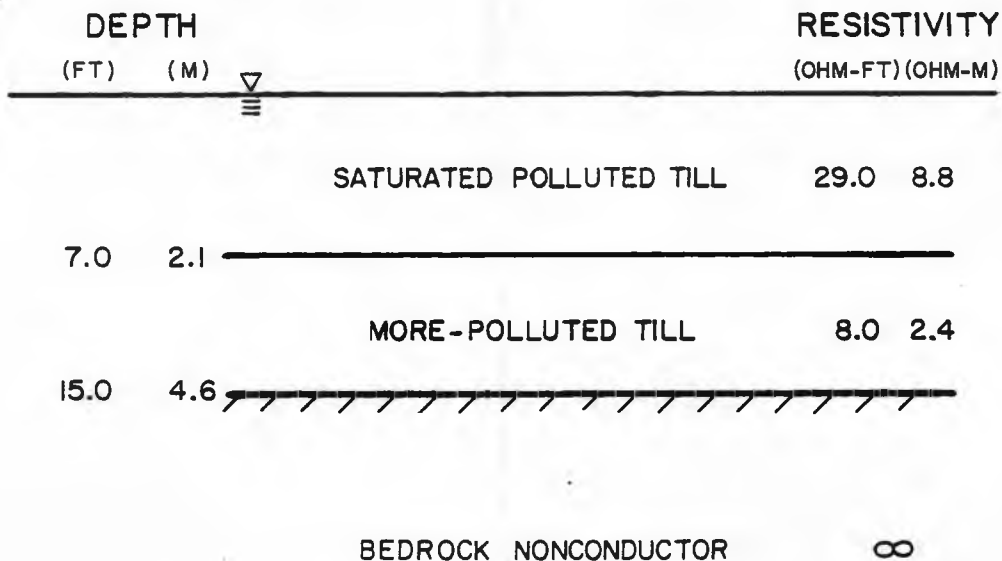
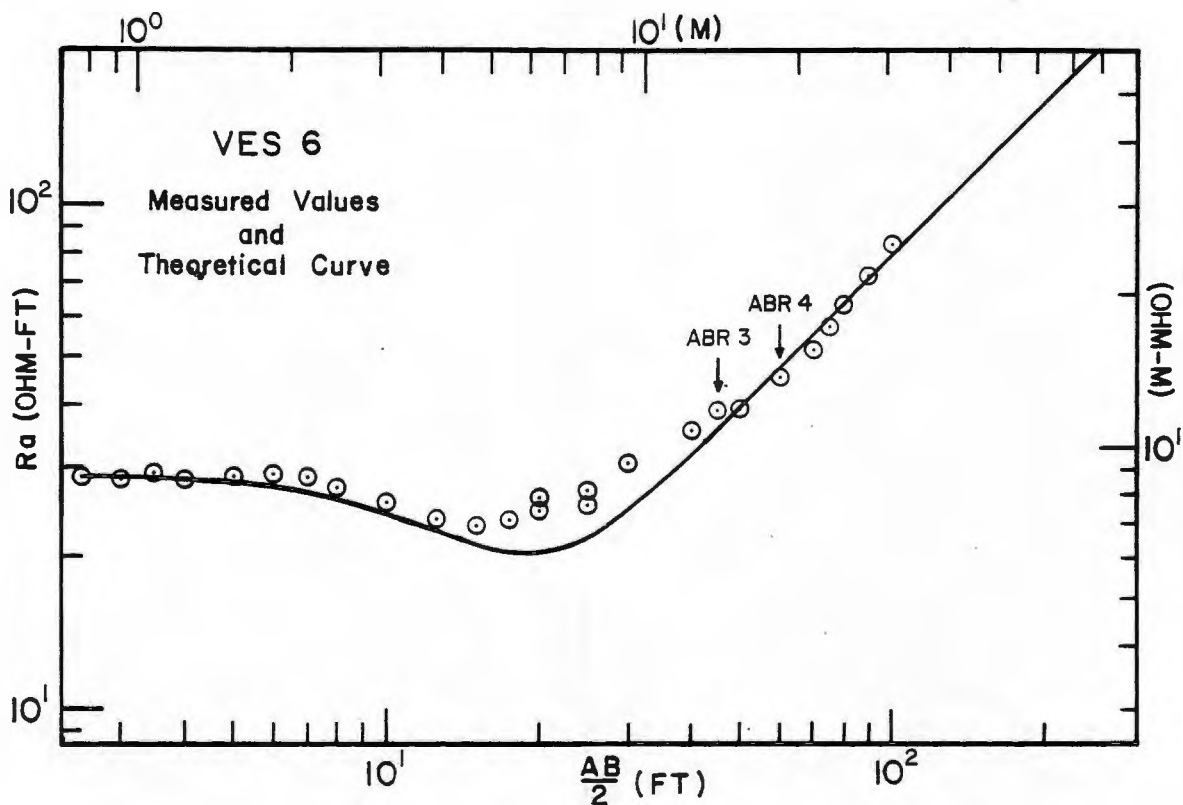


Figure 15. Field curve and geoelectric model for VES 6

The known depths to hydrogeologic boundaries were incorporated into the models for each VES as geoelectric boundaries. Other geoelectric boundaries besides the bedrock surface and the water table are somewhat arbitrary, but presumably real. According to the procedure described earlier, the bulk resistivities of the layers defined by these boundaries were varied, as were the arbitrary boundary depths to produce a best-fit curve. The values for each model were also adjusted with respect to the corresponding values in the other models, resulting in a correlated interpretation.

Only four models indicate pollution in the surficial aquifer: VES 1, 2, 3, and 6. It is important to note that the low resistivity layer, which corresponds to the intermediate minima on the field curves, lies in till above the 15ft (4.6m) depth to bedrock. The depth of 7ft (2.1m) to the top of the low resistivity layer is an arbitrary depth, but certainly falls within the limits of the principle of equivalence for each curve. The layer above the low resistivity layer also has a relatively low bulk resistivity when compared to typical resistivity values in the thousands of ohm-ft and ohm-m for other unconsolidated aquifers.

Even though till layers are often heterogeneous lithologically, the till layer at Little Compton is thought to be at least consistently heterogeneous such that a difference in lithology can be rejected as the cause of the

low resistivity layer. This assumption is supported by logs of the borehole drillings (Urish, 1980). If the boundary within the till layer is not geologic, it must necessarily be hydrogeologic, most likely resulting from a vertical transition, whether gradual or abrupt, in groundwater quality. This explanation is adequate if the means can be described for emplacement of more-polluted groundwater beneath less-polluted groundwater so close to a source area. A probable mechanism is the seasonal fluctuation of the water table within the till. During summer and fall months, the water table elevation decreases due to natural discharge, decreasing groundwater recharge from precipitation, but most importantly evapotranspiration. The loss of saturated thickness by evapotranspiration tends to concentrate the salty groundwater and restrict it to the bottom of the till layer. Evidence that the water table can fall to at least 6ft (2m) below the ground surface at Little Compton is given by Kelly and Urish (1981). During late winter and early spring, such as when the soundings were made, runoff that is salty but more dilute than the existing groundwater rapidly infiltrates the till raising the water table. The more-polluted layer within the till remains essentially undisturbed because of its higher density and because it takes mechanical dispersion a long period of time to evenly distribute the salt concentration. Consequently, the two concentrations of groundwater pollution behave as discrete geoelectric layers within a single geologic unit.

VES 2 is an exception among the models with polluted till since the normal bedrock depth was not observed. Because a boundary at a depth of 15ft (4.6m) would not produce a curve that fit the field data, the lower boundary of the more-polluted till layer was arbitrarily extended to a depth of 50ft (15.2m) in order to produce a close fit. This could indicate that a local depression in the bedrock surface was encountered or more likely that the electrical properties of the till and the shallow bedrock are locally similar. As an example, the surface of the schist bedrock may be more fractured in the vicinity of this somewhat isolated VES. This could be caused by the intersection of one or several quartz veins with the bedrock surface. Abundant cooling fractures associated with quartz veins seen in outcrops could be present allowing more of the polluted groundwater to infiltrate the bedrock than at other locations. This could cause the bulk resistivity of the fracture zone to be lowered to the resistivity of the till such that till and bedrock behave as a single geoelectric layer.

To comment briefly on why there is a discrepancy between some field points and the right-hand portion of some theoretical curves, a lateral inhomogeneity in groundwater resistivity is responsible. Evidence of the lateral inhomogeneity is given by specific conductance measurements from the two boreholes (Table 1) which indicate a definite change in groundwater resistivity within a distance of only

130ft (40m). The discrepancy is especially prominent on those soundings (VES 1, 3, and 6) which were centered over the potentially highest concentration of groundwater pollution, directly down-gradient from the salt storage shed. At small AB/2 the apparent resistivity is measured in only the highly polluted surficial material, which presents no problem. However, as AB/2 is increased the current electrodes are displaced further from the source of pollution and into areas where the groundwater pollution is more dilute in the surficial material. The effect of the lateral inhomogeneity is to increase the apparent resistivity to a value higher than would be measured if the groundwater resistivity were laterally constant. The path that the field curve would take if the pollution were laterally extensive is approximated by modeling the theoretical curve so that no field point falls more than 5% to the right of the 45° line. Thus, the discrepancy is necessary to compensate for the lateral inhomogeneity.

While only one of the polluted-till models detected any pollution below the bedrock surface, VES 4 and VES 5 demonstrate that polluted bedrock is detectable as a discrete layer beneath an unpolluted overburden. Both soundings are located to the north of the site slightly up-gradient topographically from the salt piles such that the till has not been polluted. It may at first seem unusual that pollution could be present at all in a bedrock aquifer that lies beneath an unpolluted and hydraulically

connected surficial aquifer. However, considering the high average linear velocity typical in low porosity bedrock, the anisotropy of hydraulic conductivity inherent in a fracture network, and the effects of hydrodynamic dispersion, it is entirely possible that polluted groundwater can invade the bedrock aquifer of an area without affecting the surficial aquifer. As an example, pollutants from a hazardous waste dump-site in northern Rhode Island were reported to have traveled through bedrock fractures beneath an unpolluted overburden (Goldberg-Zoino and Associates, 1981). The organic (nonmineralized) pollutants in this case were detected by chemical analysis in domestic bedrock wells remote from the waste site.

The third-layer resistivities and depths in figures 13 and 14 are medians of the ranges of practically equivalent values. The domain of practically equivalent resistivities is 113 ohm-ft (34.4 ohm-m) higher and lower than the average for VES 4 and 83 ohm-ft (25.3 ohm-m) for VES 5. At the same time the domain of practically equivalent depths is 10ft (30m) higher and lower than the average depths for both soundings. The average third-layer resistivities, 2000 ohm-ft (610 ohm-m) for VES 4 away from the salt piles and 1325 ohm-ft (404 ohm-m) for VES 5 closer to the salt piles, compare favorably with the resistivities of the salt-saturated rock samples discussed earlier. Recall that salt-saturated granite had a resistivity of 1017 ohm-ft (310 ohm-m) and salt-saturated schist had a resistivity of 623

ohm-ft (190 ohm-m).

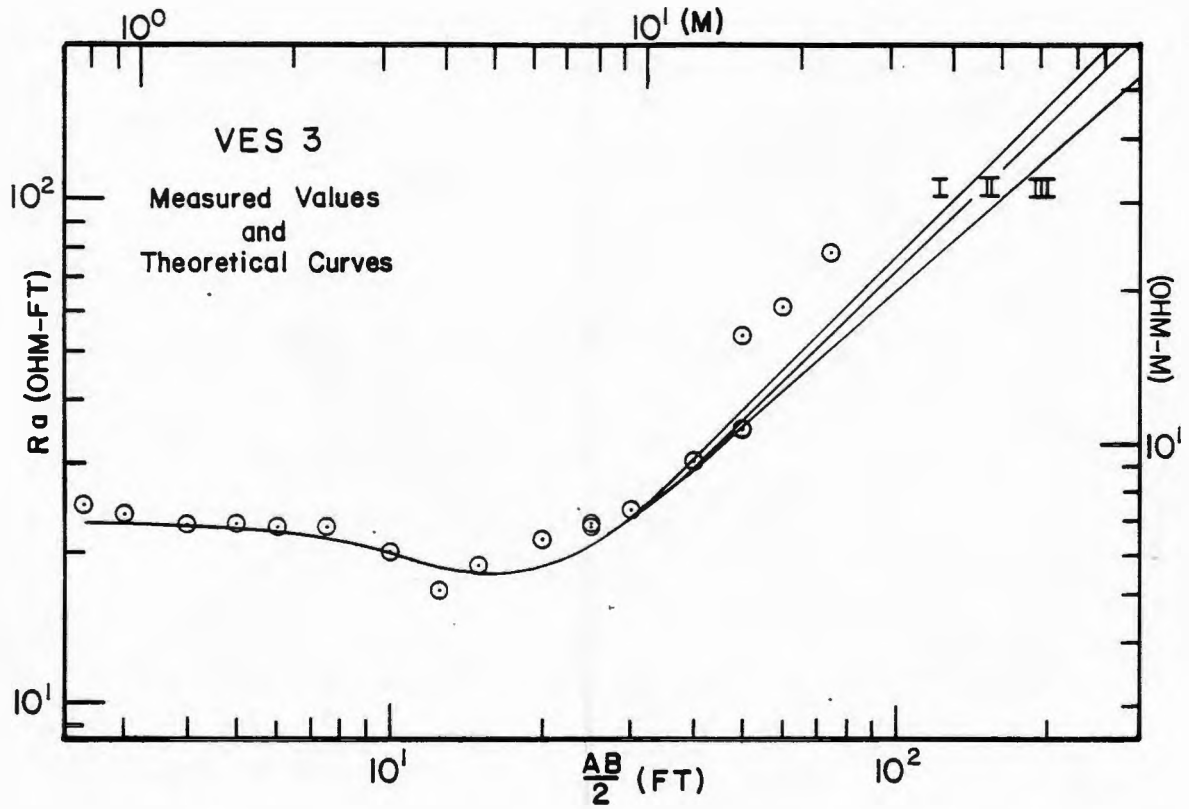
While the third-layer resistivity values from Little Compton are slightly higher than the resistivity values measured in "polluted" rock samples, they remain considerably lower than the resistivity value of 27,880 ohm-ft (8500 ohm-m) measured in the "unpolluted" granite sample. Since the minerals in both the rock and bedrock samples are essentially non-conductive, discrepancies between field values and laboratory values are attributable to differences in physical conditions during measurement. The pressure applied to the rock samples is higher than the pressure in shallow bedrock and thus decreased the interconnected pore volume. A decrease in porosity, however, favors an increase in resistivity, which is contrary to the results above. Therefore, the saturating fluid quality must be the factor above all else that controls the bulk resistivity of these materials. Since the porewater resistivity was lower in the rock samples and the temperature was higher, the bulk resistivity of the rock samples would be expected to be lower than the bulk resistivity of the bedrock at Little Compton. Thus, it can be concluded with confidence that the third-layer resistivity values from VES 4 and 5 are reasonable values for polluted fractured bedrock.

Since polluted bedrock was interpreted from two field curves in an area not expected to be detectably polluted, a question is raised as to why the most-polluted bedrock was



not represented on the other field curves. The principle of suppression provides an explanation. The surficial layers of VES 1, 3, and 6 have very low resistivities compared to the polluted bedrock resistivities obtained by VES 4 and 5. Subsequently, the polluted bedrock layer, even though greatly reduced in resistivity from unpolluted bedrock, still behaves as a nonconductor relative to the even lower resistivity overburden. The suppression of the polluted bedrock layer at Little Compton makes its thickness and resistivity uninterpretable in areas of highly polluted till.

To illustrate the extent of the suppression phenomenon, two hypothetical models for VES 3 are presented in figure 16. Model I is the correlated model of figure 12 presented here for comparison. Model II is identical to Model I except that the third layer thickness and resistivity of VES 5 has been added to simulate a polluted bedrock layer. As can be seen, the curve generated by Model II is practically coincident to the curve of Model I. Model III represents an extreme case of Model II where the polluted bedrock layer has a bulk resistivity of 500 ohm-ft (152.4 ohm-m) and a thickness of 300ft (91.4m). However, the curve generated by Model III is also practically coincident making Models I, II, and III practically equivalent at least to the maximum values of  $AB/2$  that were performed. Since it is known from the borehole data that the bedrock at this VES location is polluted, it can be stated that the polluted bedrock layer



MODEL I (same as Figure 12)

7 ft		15 ft		
23.0 ohm-ft	8.0	$\infty$		
7.0 ohm-m	2.4			
2.1 m		4.6 m		

MODEL II

7 ft		15 ft		175 ft	
23.0 ohm-ft	8.0	1325		$\infty$	
7.0 ohm-m	2.4	404			
2.1 m		4.6 m		53.3 m	

MODEL III

7 ft		15 ft		315 ft	
23.0 ohm-ft	8.0	500		8	
7.0 ohm-m	2.4	152			
2.1 m		4.6 m		96.0 m	

Figure 16. Theoretical models of third-layer suppression

is suppressed on the field curve. It would have been impossible to say whether or not pollution exists in the bedrock aquifer at this location based on the VES interpretation alone. A general conclusion reached from these results is that unless the overburden resistivity is of the same magnitude as the polluted bedrock resistivity, the polluted bedrock layer will be suppressed beyond recognition on the field curve.

#### Application of formation factor and Archie's law

The formation factor of the bedrock at Little Compton can be calculated using the bulk resistivity from VES 5 and the groundwater resistivity from borehole LIC 21 nearby. Dividing the polluted bedrock resistivity of 1325 ohm-ft (404 ohm-m) by the groundwater specific conductance expressed as a resistivity of 17.3 ohm-ft (5.3 ohm-m), the formation factor is found to be 77 (equation 4). This value is low compared to the formation factors of 1017 and 760 calculated respectively for the salt-saturated Westerly granite and chlorite schist rock samples discussed previously. Surface conductance and clay mineral ionization are not responsible for the discrepancy because their effects are minimal in salt-saturated rocks. For this reason all three formation factors can be considered true rather than apparent formation factors. The discrepancy may

be explained by the lowered porosity of the rock samples which were under 50 times atmospheric pressure during resistivity measurement. Since there is an inverse relationship between porosity and formation factor (equation 6), the lower-porosity rock samples would be expected to have higher formation factors. While few formation factors for crystalline rock are found in the literature, statistical studies have been performed on numerous samples of sandstone. One such study by Carothers (1968) reports that values vary from 5 to more than 1000 in 793 sandstone samples, making it likely that crystalline bedrock varies as much. The formation factor of 77 derived for the schist bedrock at Little Compton appears to be reasonable.

The bedrock groundwater resistivity can be calculated at VES 4, which is the sounding farthest away from the pollution source and also farthest north. The polluted bedrock resistivity of 2000 ohm-ft (610 ohm-m) is this time divided by the derived formation factor of 77 to obtain a groundwater resistivity of 26 ohm-ft (7.9 ohm-m). This translates into a specific conductance of 1260 micromhos/cm which is still several times higher than the conductivity of the natural groundwater. Using Keys and MacCary's nomogram (1971), the groundwater at VES 4 has an approximate salinity of 1000 mg/l compared to a salinity of 1500 mg/l at VES 5. Groundwater pollution is therefore confirmed at both VES locations and an expected decrease in salinity is demonstrated away from the pollution source.

A typical expression of Archie's law for metamorphosed sedimentary rock is given by Keller (1967) as

$$R_w / R_i = 1.4 n^{-1.58} \quad (9)$$

Since  $R_w/R_i$  is the formation factor, now known to be 77, the equation can be solved for porosity ( $n$ ). A value of 7.9% is obtained which represents the total porosity of the bedrock. The schist bedrock at Little Compton must contain a large amount of intergranular porosity since joint porosity rarely exceeds 2%. However, much of the intergranular porosity measured from electrical current flow may not be accessible to groundwater flow. Therefore, the porosity calculated by Archie's law for bedrock is likely an overestimate of effective porosity and should be considered as such when used in groundwater equations.

A groundwater flow equation that utilizes porosity to determine the rate of pollution transport was given earlier as equation 7. If the entire polluted bedrock thickness is considered to be a large enough scale of homogeneity, equation 7 can be applied to the fractured medium as an equivalent granular medium. Besides a value for effective porosity, values for bulk hydraulic conductivity and hydraulic gradient are needed in order to calculate average linear velocity. In many groundwater studies the latter two values are measured by bail or slug tests and by water level measurements in at least three bedrock wells. Effective

porosity is often the value that is difficult to obtain. A porosity derived by VES curve interpretation and Archie's law may be used as the effective porosity in equation 7, but only with caution. Besides the likelihood that it overestimates the effective porosity, the porosity value is only as accurate as the VES curve interpretation and the parameters used for Archie's law. Unfortunately for the present study, only a rough approximation of porosity is known.

To demonstrate a result that can be achieved using equation 7, an estimate of the average linear velocity of pollution flow through the bedrock aquifer at Little Compton will be calculated. Freeze and Cherry (1979) indicate that hydraulic conductivity values for fractured igneous and metamorphic rocks range from slightly less than  $10^{-8}$  m/s ( $32.8^{-8}$  ft/s) to slightly more than  $10^{-4}$  m/s ( $32.8^{-4}$  ft/s). An average value of  $10^{-6}$  m/s ( $32.8^{-6}$  ft/s) will be used. When water levels from three boreholes are available, the direction of groundwater flow and the hydraulic gradient in that direction can be determined by triangulation. Not having three bedrock boreholes available for measurement at Little Compton, a commonly observed field value for hydraulic gradient of  $10^{-2}$  will be assumed (Freeze and Cherry, 1979). Using these values and the porosity of 7.9% in equation 7, an average linear velocity of 4 m/year or 13 ft/year is computed. Realizing this is only a very rough estimate, it is at least a sufficient rate to have carried

the leading boundary of pollution to the location of VES 4 in only 14 years.

The groundwater flow system at Little Compton is complicated by the site's location on a topographic divide. More than one direction of groundwater flow may occur even in the bedrock aquifer, making an estimation of average linear velocity difficult to apply. It may be that water in the subsurface flows away in all directions causing the bedrock pollution to surround the site. Since soundings could not be performed away from the site to the east, south, and west because of physical obstructions, it cannot be determined if pollution has spread as far in those directions as it has to the north. If by chance the pollution has spread farther towards VES 4 than in any other direction, it may have resulted from either the fracture orientation favoring hydraulic conductivity in that direction or mechanical dispersion operating faster than advection in that direction. Despite the complications involved in applying the groundwater flow equation, VES curve interpretation has not only successfully detected pollution in a bedrock aquifer in an area that otherwise may have been presumed to be unpolluted, but also has facilitated the quantitative description of the degree of pollution.

## AB Rectangle Mapping

### Instrumentation and measurement locations

The same instrumentation described for vertical electrical soundings was used to perform AB rectangle mapping. Each rectangle at Little Compton was 20ft (6m) square containing a grid pattern of 25 measuring points. Four AB rectangles were made at the Little Compton site at the locations shown in figure 17. One (ABR 1) was centered at VES 5 with an AB/2 of 175ft (53m) while another (ABR 2) was centered at VES 3 with an AB/2 of 30ft (9m). Two more (ABR 3 and ABR 4) were made near the latter, centered at VES 6 with AB/2 values of 45ft (14m) and 60ft (18m). Contour maps of the normalized residual resistivities are presented in figures 18-21 for ABR 1-4, respectively. The measured resistivity values and their coordinates in relation to the center point are listed in Appendix D.



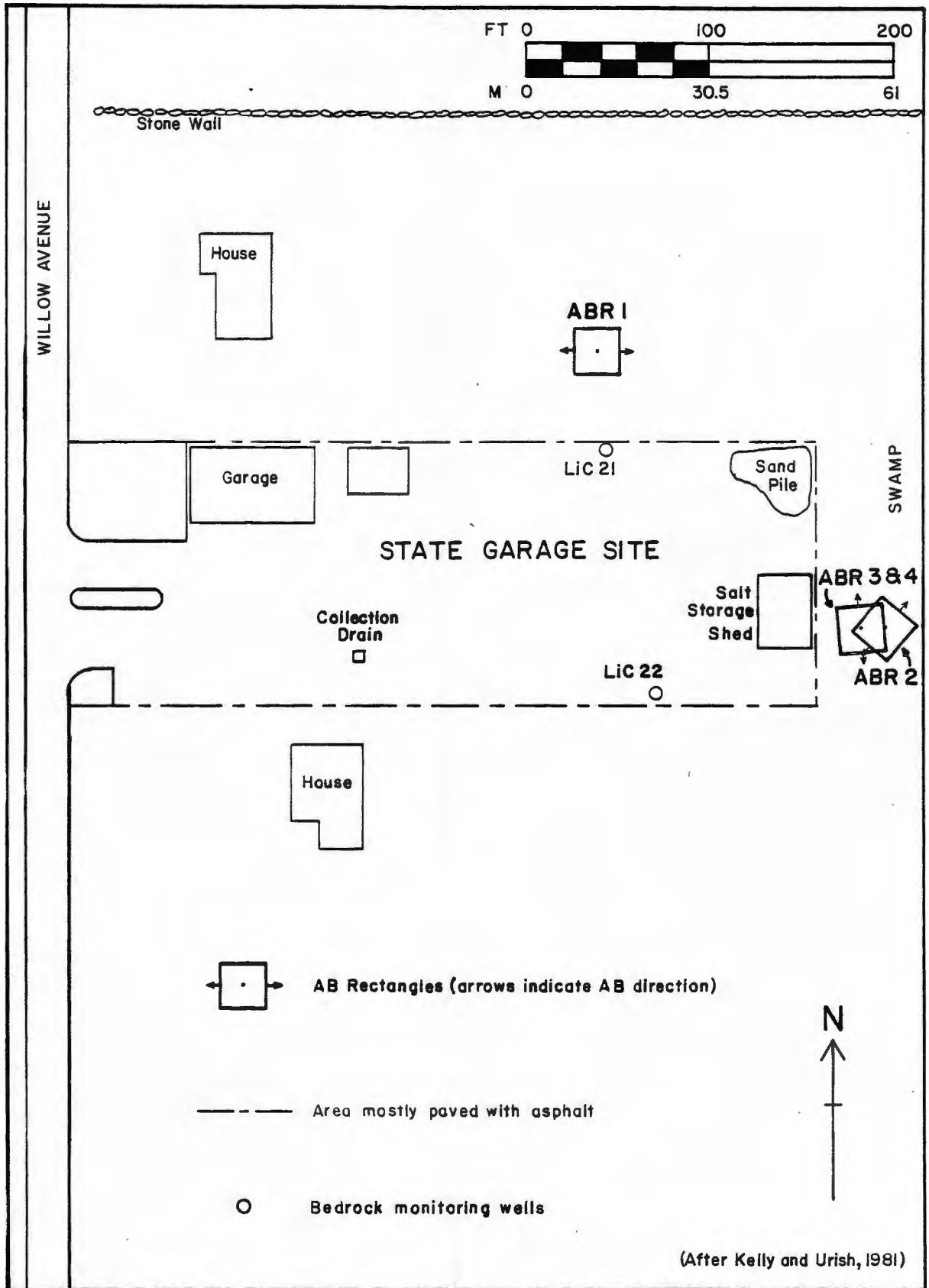


Figure 17. Location map of AB Rectangles

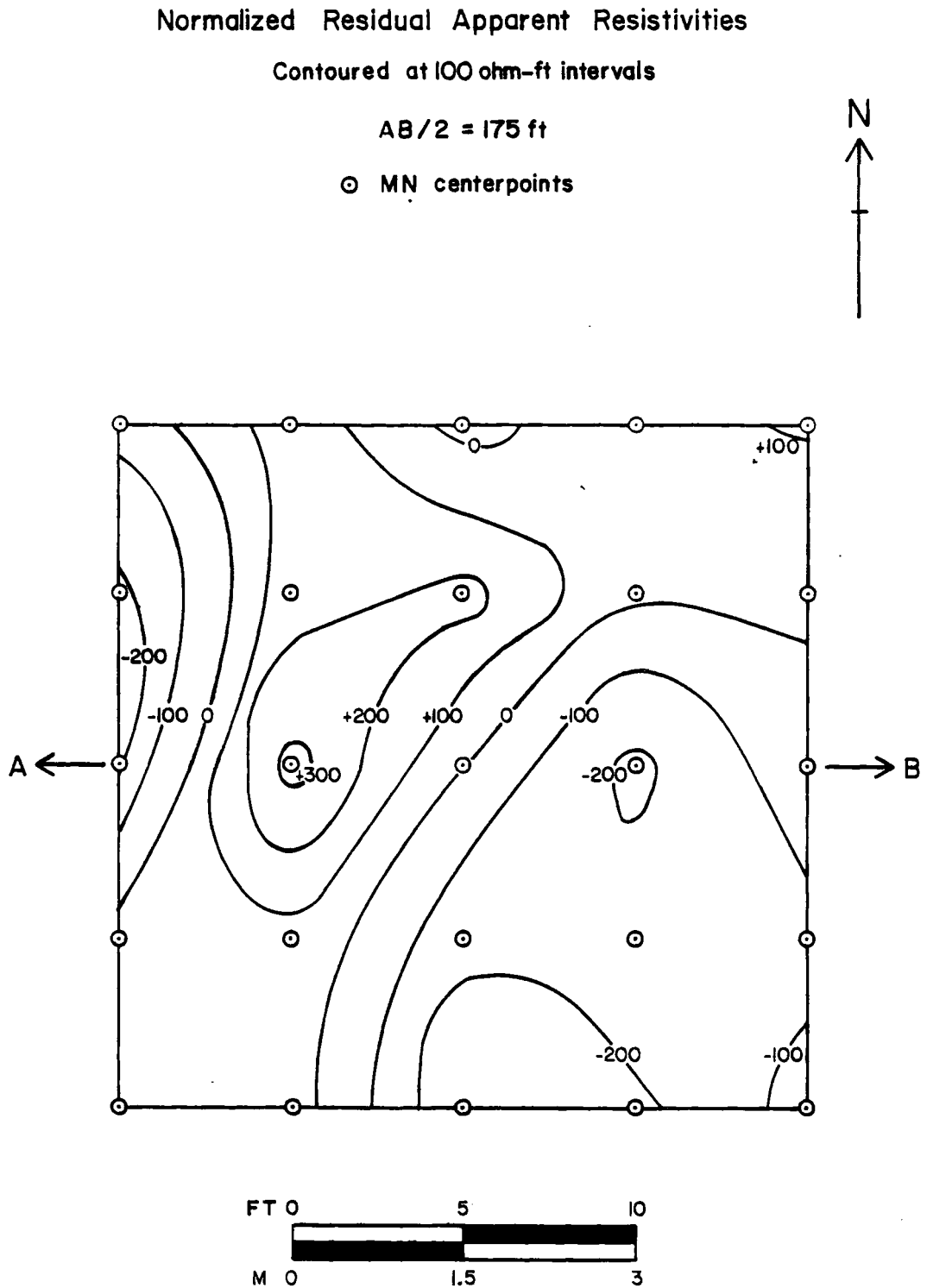


Figure 18. Resistivity contour map for ABR 1

### Normalized Residual Apparent Resistivities

Contoured at 5 ohm-ft intervals

$$AB/2 = 30 \text{ ft}$$

⊙ MN centerpoints

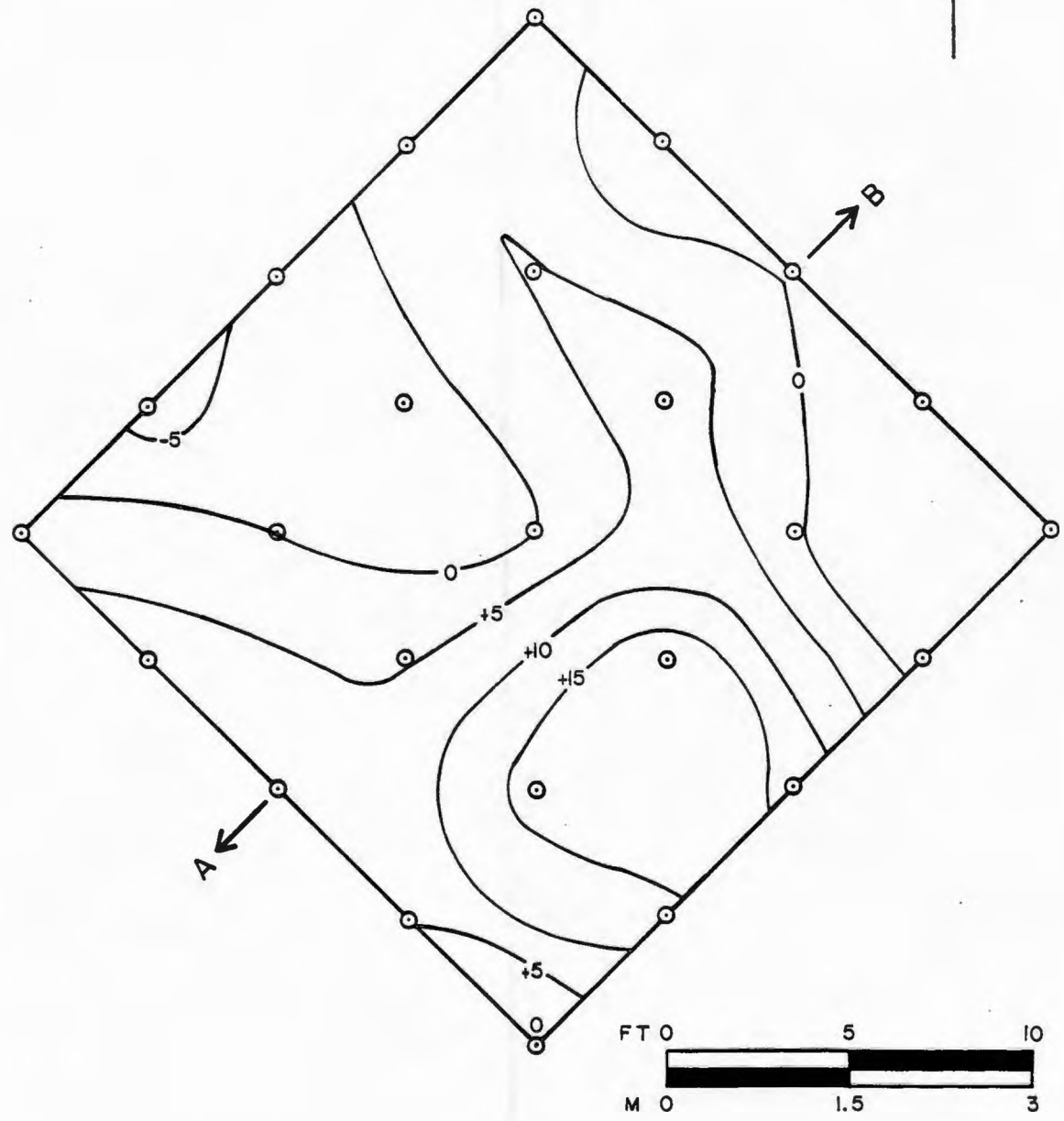


Figure 19. Resistivity contour map for ABR 2

### Normalized Residual Apparent Resistivities

Contoured at 5 ohm-ft intervals

AB/2 = 45 ft

⊙ MN centerpoints

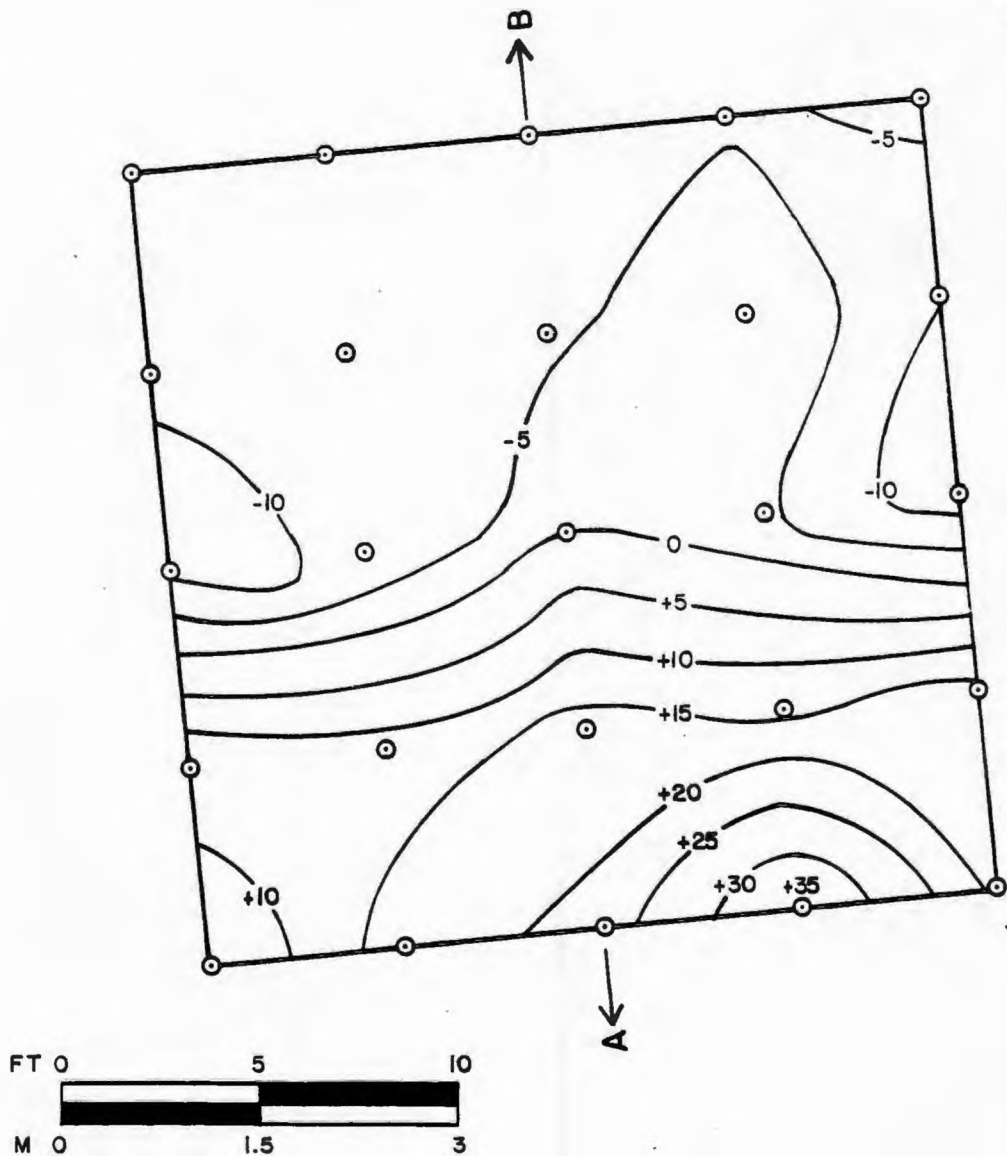


Figure 20. Resistivity contour map for ABR 3

### Normalized Residual Apparent Resistivities

Contoured at 5 ohm-ft intervals

$AB/2 = 60$  ft

⊙ MN centerpoints

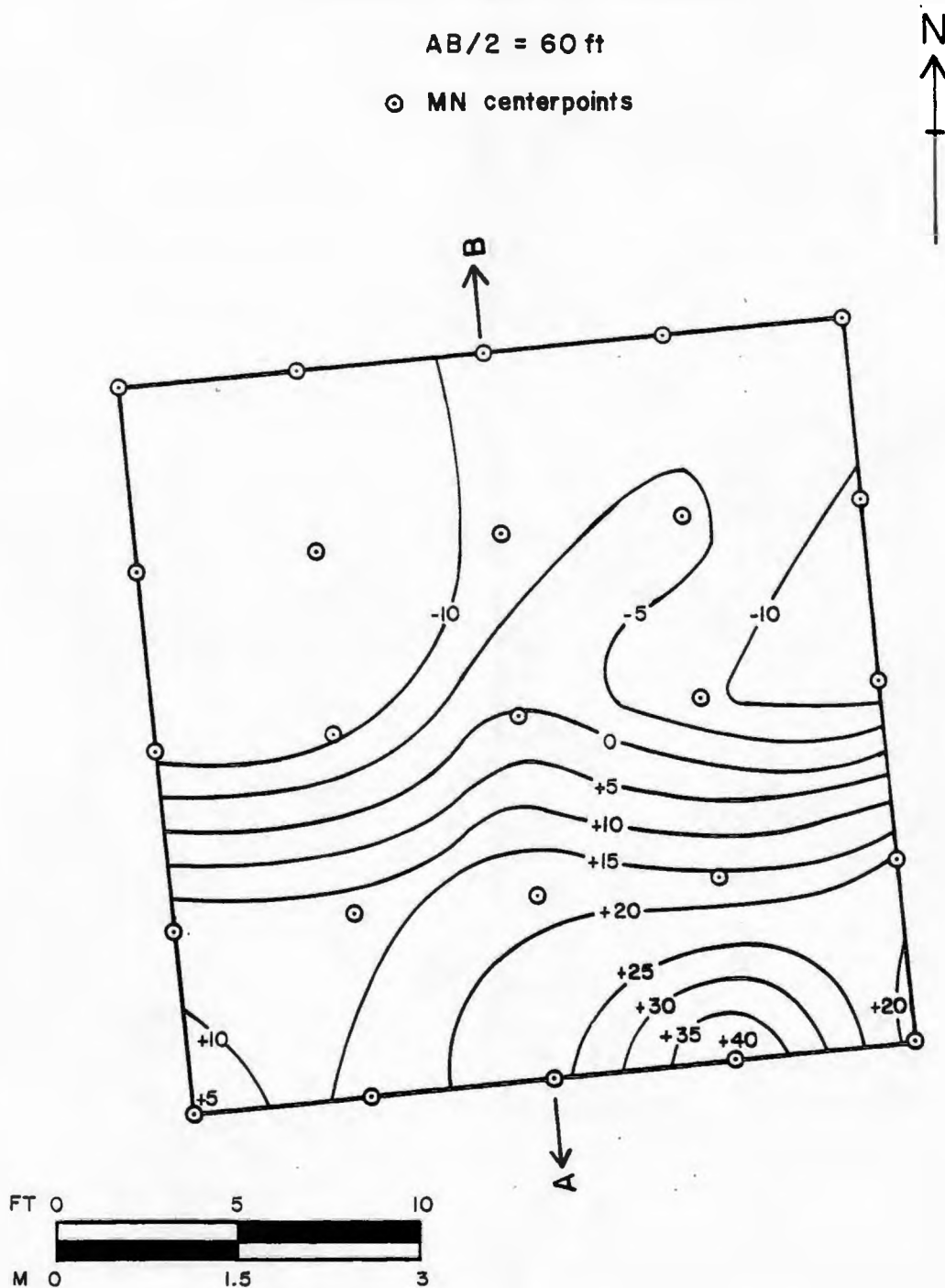


Figure 21. Resistivity contour map for ABR 4

## Discussion of results

The arrows in figures 12, 14, and 15 indicate where each AB rectangle center point falls on its respective VES curve. Note that all four center points lie on the right-hand rising portion of the curves assuring that each rectangle is penetrating at least some thickness of bedrock. Note also that ABR 1 is the only rectangle located over unpolluted till. The thickness of polluted bedrock penetrated by this rectangle is much greater than the thickness penetrated by the other three rectangles since the  $AB/2$  value is much larger. Judging from the interpretation of VES 5, apparent resistivity is being measured by ABR 1 through a thickness of more than 175ft (53m) of which only 15ft (4.6m) is till. Therefore, the values of apparent resistivity can be interpreted as being almost exclusively contributed by the bedrock. Conversely, the other three AB rectangles are located over polluted till which means that their interpretations of bedrock pollution may be influenced by the same masking effect that plagues the VES interpretations in polluted till.

Recall that the contour values in figures 18-21 do not represent actual apparent resistivities, but rather variations of measured resistivity values from expected, theoretically derived values. The expected value at any grid point is a median value predicted by the trace of the

corresponding theoretical VES curve. Thus, some of the contour values are above the predicted median (positive values) while others are below the predicted median (negative values). The sign of the contours has also been affected by the normalizing of each grid point value to give the center point a value of zero variation. Therefore, the contour values are relative not only to predicted medians, but also to the center point value.

Having reduced the AB rectangle measurements to contours of points with equal value, interpretations of bedrock pollution can be made from the the maps. The areas of ABR 1 in figure 18 with negative values to the west and to the southeast probably represent a local zone of fractures, or perhaps one particularly wide fracture, filled with low-resistivity polluted groundwater. Just west of the center is an area with positive values indicating relatively solid rock. The northeastward elongation of these areas serves to substantiate the interpretation since the strike of fractures in outcrops is also northeastward. One way to confirm the interpretation would be to drill test holes at the locations of the most positive and most negative values on the map. If the hole in the area of negative values yielded water while the other hole yielded little or no water, the AB rectangle method could likely be used to locate other wells for monitoring pollution movement in the bedrock aquifer. With further research the method could prove to be an accurate technique for locating a bedrock

well where it will intercept an optimum number of water-bearing fractures, even in unpolluted fractured bedrock.

The results of ABR 2, 3, and 4 are less convincing than the results of ABR 1 because the thickness of bedrock relative to the thickness of till through which apparent resistivity was measured is much less. Also, interpretations of the corresponding VES curves show that the till has a much lower resistivity than the polluted bedrock which may adversely affect the interpretation of map anomalies as fracture patterns in the bedrock. Since the center points of ABR 2, 3, and 4 were nearly coincident and only the orientations of the rectangles and their depths of measurement are different, the rectangle maps can be compared to each other once oriented and overlapped as in figures 19-21. It can be seen that the areas of positive and negative values coincide from one map to another. The continuity between maps could indicate either the continuation of fractures with depth or the overriding effects of lateral variations of resistivity in the polluted till which are masking any variations in the bedrock. Since the northeastward trend of the contours in these three maps is more subtle than in the map for ABR 1, it may be that the contour pattern is being established by the till layer and not by the bedrock. The fact that the contour interval is 5 units for these maps compared to 100 units for the ABR 1 map tends to support this interpretation. However, with only



these measurements available, it is difficult to accurately assess the effectiveness of AB rectangle mapping for detecting bedrock pollution below polluted overburden. Once again, further research is necessary.

## SUMMARY

1. A 15ft (4.6m) thickness of jointed till is transmitting salt-polluted runoff into fractured crystalline bedrock at the Little Compton site. Two geoelectrically distinct layers have been interpreted within the till below the water table and are thought to be caused by a difference in the salinity of the groundwater rather than by a difference in the lithology.
  
2. Although the bedrock beneath the Little Compton site was originally mapped as Bulgarmarsh Granite, bedrock boreholes in the vicinity indicate the bedrock is actually mica-chlorite schist. Several joint sets observable in outcrops make the bedrock an effective conductor of groundwater.
  
3. In an area of unpolluted till, polluted bedrock has been interpreted from two vertical electrical soundings as a discrete layer. The VES curve interpretations indicate that polluted groundwater has travelled faster through the bedrock fractures than through the overlying till. Additionally, the pollution is penetrating deeper into the bedrock and becoming more dilute as it moves farther from the source.

4. The principle of suppression explains why the polluted bedrock layer was uninterpretable from vertical electrical soundings in areas of polluted till. If the surficial layers have bulk resistivities much lower than the bulk resistivity of the polluted bedrock, the bedrock pollution likely will not be detectable.
  
5. While the horizontal profiling and AB rectangle mapping measurements in polluted till did not provide conclusive evidence of bedrock pollution, an AB rectangle map over unpolluted till apparently shows the pattern of pollution-filled fractures. AB rectangle mapping is a promising method for placing bedrock monitoring wells and deserves further research.

## REFERENCES CITED

- Archie, G.E., 1942, The electrical resistivity log as an aid in determining some reservoir characteristics: Trans. AIMME, v. 146, p. 54-62.
- Beissel, D.R., 1971, Geophysical studies of fractured rock [M.S. thesis]: Ft. Collins, Colorado, Colorado State University, 53 p.
- Benedini, M., 1976, The aquifers and their hydraulic characteristics: Geoexploration, v. 14, p. 157-178.
- Bhattacharya, P.K., and Patra, H.P., 1968, Direct current geoelectric sounding: Amsterdam, Elsevier Publishing Co., 135 p.
- Billings, M.P., 1972, Structural geology (3rd ed.): Englewood Cliffs, New Jersey, Prentice-Hall, Inc., 606 p.
- Brace, W.F., and Orange, A.S., 1968, Further studies of the effects of pressure on electrical resistivity of rocks: Journal of Geophysical Research, v. 73, no. 16, p. 5407-5420.
- Brace, W.F., Orange, A.S., and Madden, T.R., 1965, The effect of pressure on the electrical resistivity of water-saturated crystalline rocks: Journal of Geophysical Research, v. 70, no. 22, p. 5669-5678.
- Brace, W.F., and others, 1972, Cracks and pores: a closer look: Science, v. 178, p. 162-163.

- Breusse, J.-J., 1963, Modern geophysical methods for subsurface water exploration: *Geophysics*, v. 28, no. 4, p. 633-657.
- Carothers, J.E., 1968, A statistical study of the formation factor relation: *The Log Analyst*, Sept.-Oct., p. 13-20.
- Cushman, R.V., Allen, W.B., and Pree, H.L., Jr., 1953, Geologic factors affecting the yield of rock wells in southern New England: reprint from *Journal of the New England Water Works*, v. 67, no. 2, p. 77-95.
- Davis, S.N., 1969, Porosity and permeability of natural materials: in De Wiest, R.J.M., ed., *Flow through porous media*: New York, Academic Press, p. 53-89.
- Davis, S.N., and De Wiest, R.J.M., 1966, *Hydrogeology*: New York, John Wiley and Sons, 463 p.
- Feininger, T., 1971, Chemical weathering and glacial erosion of crystalline rocks and the origin of till: U.S. Geological Survey Professional Paper 750-C, p. 65-81.
- Fetter, C.W., 1980, *Applied hydrogeology*: Columbus, Ohio, Charles E. Merrill Publishing Co., 488 p.
- Freeze, R.A., and Cherry, J.A., 1979, *Groundwater*: Englewood Cliffs, New Jersey, Prentice-Hall, Inc., 604 p.
- Frohlich, R.K., 1973, Detection of fresh water aquifers in the glacial deposits of northwestern Missouri by geoelectrical methods: *Water Resources Bulletin*, v. 9, no. 4, p. 723-734.

- Goldberg-Zoino and Associates, Inc., 1981, Bedrock water contamination study, Burrillville, Rhode Island: prepared for R.I. Department of Environmental Management, 8 p.
- Greenberg, R.J., and Brace, W.F., 1969, Archie's law for rocks modeled by simple networks: Journal of Geophysical Research, v. 74, no. 8, p. 2099-2102.
- Heath, R.C., and Trainer, F.W., 1981, Introduction to ground water hydrology: Worthington, Ohio, Water Well Journal Publishing Co., 285 p.
- Hobbs, B.E., Means, W.D., and Williams, P.F., 1976, An outline of structural geology: New York, John Wiley and Sons, Inc., 571 p.
- Keller, G.V., 1967, Application of resistivity methods in mineral and groundwater exploration programs: in Mining and Groundwater Geophysics / 1967, Economic Geology Report No. 26, Geological Survey of Canada, 722 p.
- Keller, G.V., and Frischknecht, F.C., 1966, Electrical methods in geophysical prospecting: Oxford, Pergamon Press, 519 p.
- Kelly, W.E., 1976, Geoelectric sounding for delineating ground water contamination: Ground Water, v. 14, no. 1, p. 6-10.

- Kelly, W.E., and Urish, D.W., 1981, A study of the effects of salt storage practices on surface and ground water quality in Rhode Island: Federal Highway Administration Report FHWA-RI-RD-80-01, U.S. Department of Transportation, 54 p.
- Keys, W.S., and MacCary, L.M., 1971, Application of borehole geophysics to water-resources investigations: Techniques of Water-Resources Investigations of the U.S. Geological Survey, bk. 2, ch. E1, 126 p.
- Klefstad, G., Sandlein, L.V.A., and Palmquist, R.C., 1975, Limitations of the electrical resistivity method in landfill investigations: Ground Water, v. 13, no. 5, p. 418-427.
- Koefoed, O., 1979, Geosounding principles, 1: resistivity sounding measurements: Amsterdam, Elsevier Scientific Publishing Co., 276 p.
- Kowalski, R.G., and Sanders, D.S., 1983, Introduction to hydrogeologic investigations of contamination in fractured rock: R.I. Water Resources Center Technical Report No. 13, 71 p.
- Kunetz, G., 1966, Principles of direct current resistivity prospecting: Berlin, Geopublication Associates, 103 p.
- Madden, T.R., 1976, Random networks and mixing laws: Geophysics, v. 41, no. 6A, p. 1104-1125.
- Pollock, S.J., 1964, Bedrock geology of the Tiverton quadrangle Rhode Island-Massachusetts: U.S. Geological Survey Bulletin 1158-D, 16 p.

- Satpathy, B.N., and Kanungo, D.N., 1976, Groundwater exploration in hard-rock terrain - a case history: Geophysical Prospecting, v. 24, no. 4, p. 725-736.
- Schiner, G.R., and Gonthier, J.B., 1965, Ground-water map of the Tiverton and Sakonnet Point quadrangles, Rhode Island, and the Rhode Island portion of the Westport quadrangle, Massachusetts: R.I. Water Resources Coordinating Board in cooperation with U.S. Geological Survey, GWM 21.
- Shankland, T.J., and Waff, H.S., 1974, Conductivity in fluid-bearing rocks: Journal of Geophysical Research, v. 79, no. 32, p. 4863-4868.
- Shipman, W.D., 1978, Saltwater-bearing aquifers at the periphery of Narragansett Bay: geoelectric and geohydrologic characteristics [M.S. thesis]: Kingston, Rhode Island, University of Rhode Island, 103 p.
- Spencer, E.W., 1977, Introduction to the structure of the earth (2nd ed.): New York, McGraw-Hill Book Co., 640 p.
- Stollar, R.L., and Roux, P., 1975, Earth resistivity surveys - a method for defining ground-water contamination: Ground Water, v. 13, no. 2, p. 145-150.
- Unz, M., 1953, Apparent resistivity curves for dipping beds: Geophysics, v. 18, p. 116-137.
- 1968, Vertical profiling over a medium of continuously varying resistivity: Geophysical Prospecting, v. 16, p. 427-435.



Urish, D.W., 1980, Personal Notes.

\_\_\_\_\_, 1983, The practical application of surface electrical resistivity to detection of ground-water pollution: *Ground Water*, v. 21, no. 2, p. 144-152.

U.S. Geological Survey, 1963, Open-file well reports: Providence, Rhode Island, Water Resources Division.

Van Nostrand, R.G., and Cook, K.L., 1966, Interpretation of resistivity data: U.S. Geological Survey Professional Paper 499, 310 p.

Verma, R.K., Rao, M.K., and Rao, C.V., 1980, Resistivity investigations for ground water in metamorphic areas near Dhanbad, India: *Ground Water*, v. 18, no. 1, p. 46-55.

Warner, D.L., 1969, Preliminary field studies using earth resistivity measurements for delineating zones of contaminated ground water: *Ground Water*, v. 7, no. 1, p. 9-16.

Williams, R.E., and Farvolden, R.N., 1969, The influence of joints on the movement of groundwater through glacial till: *Journal of Hydrology*, v. 5, p. 163-170.

Witherspoon, P.A., 1981, Effect of size on fluid movement in rock fractures: *Geophysical Research Letters*, v. 8, no. 7, p. 659-661.

Zartman, R.E., and Naylor, R.S., in press, Structural implications of some radiometric ages of igneous rocks in southeastern New England: *Geological Society of America Bulletin*.

Zohdy, A.A.R., Eaton, G.P., and Mabey, D.R., 1974, Application of surface geophysics to ground-water investigations: Techniques of Water-resources Investigations of the U.S. Geological Survey, bk. 2, ch. D1, 116 p.

Zumberge, J.H., and Nelson, C.A., 1976, Elements of physical geology: New York, John Wiley and Sons, Inc., 395 p.

## APPENDIX A. Fortran Program for Computing K-factors

```

100  10  FORMAT(' A PROGRAM TO CALCULATE THE GEOMETRIC')
110  20  FORMAT(' FACTOR (K) FOR AB RECTANGLE MAPPING')
120  30  FORMAT(' OVALUES MUST BE ENTERED IN FORMAT 00.0')
130  40  FORMAT(' OENTER AB/2 VALUE')
140  50  FORMAT(F5.1)
150  60  FORMAT(' OENTER MN VALUE')
160  70  FORMAT(F4.1)
170  80  FORMAT(' OENTER LATERAL DISP. (X): 99.0 TO STOP')
180  90  FORMAT(' OENTER DISP. TOWARDS A OR B (Y)')
190 100  FORMAT(' OK='F10.2)
200 110  FORMAT(' OENTER 1 TO CHANGE AB/2 AND MN')
210 120  FORMAT(I1)
220      REAL AM, BM, AN, BN, K, Z, MN, X, Y
230      INTEGER Q
240      WRITE(6,10)
250      WRITE(6,20)
260      WRITE(6,30)
270 130  WRITE(6,40)
280      READ(5,50) Z
290  "NOTE: Z=AB/2
300      WRITE(6,60)
310      READ(5,70) MN
320 140  WRITE(6,80)
330      READ(5,70) X
340      IF(X.EQ.99.0) GOTO 150
350      WRITE(6,90)
360      READ(5,70) Y
370      AM=((Z+X-MN/2)**2+Y**2)**(-.5)
380      BM=((Z-X+MN/2)**2+Y**2)**(-.5)
390      AN=((Z+X+MN/2)**2+Y**2)**(-.5)
400      BN=((Z-X-MN/2)**2+Y**2)**(-.5)
410      K=6.283/(AM-BM-AN+BN)
420      WRITE(6,100) K
430      GOTO 140
440 150  WRITE(6,110)
450      READ(5,120) Q
460      IF(Q.EQ.1) GOTO 130
470      STOP
480      END

```

## APPENDIX B. Horizontal Profiling Field Data

Table 2. Field Data for W to E Horizontal Profile Line

Station	A-Spacing		I (ma)	V (mv)	Ra	
	(ft)	(m)			(ohm-ft)	(ohm-m)
A	50	15.2	83	31.5	119.2	36.3
B	50	15.2	29	15.8	171.2	52.2
C	50	15.2	100	64.7	203.3	62.0
D	75	22.9	210	143.5	321.8	98.1
E	50	15.2	180	144.8	252.7	77.0
F	75	22.9	165	83.0	236.9	72.2
G	50	15.2	42	24.2	181.0	55.2
H	50	15.2	110	75.65	216.1	65.9
I	75	22.9	140	75.0	252.4	76.9
J	50	15.2	200	39.15	61.5	18.7
K	50	15.2	140	40.6	91.1	27.8

Table 3. Field Data for N to S Horizontal Profile Line

Station	A-Spacing		I (ma)	V (mv)	Ra	
	(ft)	(m)			(ohm-ft)	(ohm-m)
A	50	15.2	37	141.5	1201.4	366.2
B	75	22.9	37	56.1	714.5	217.8
C	50	15.2	31	33.35	338.0	103.0
D	50	15.2	42	25.45	190.4	58.0
E	75	22.9	39.5	11.55	137.8	42.0
F	50	15.2	220	58.0	82.8	25.2

## APPENDIX C. Vertical Electrical Sounding Field Data

Table 4. Field Data for VES 1 (4/1/83)

AB/2		MN		I (ma)	V (mv)	Ra	
(ft)	(m)	(ft)	(m)			(ohm-ft)	(ohm-m)
2.5	0.8	1	0.3	149	52.5	6.6	2.1
4	1.2	1	0.3	149	26.0	8.6	2.6
6	1.8	1	0.3	148	13.5	10.2	3.1
8	2.4	1	0.3	148	8.5	11.5	3.5
10	3.0	1	0.3	148	5.8	12.3	3.8
15	4.6	1	0.3	147	2.4	11.5	3.5
25	7.6	1	0.3	147	0.8	10.7	3.3
25	7.6	4	1.2	147	3.5	11.6	3.5
40	12.2	4	1.2	130	1.55	14.9	4.5
65	19.8	4	1.2	140	0.85	20.1	6.1
65	19.8	8	2.4	138	1.7	20.4	6.2
100	30.5	8	2.4	67.5	0.75	43.6	13.3
125	38.1	8	2.4	74.5	0.65	53.5	16.3
125	38.1	20	6.1	74.5	1.7	55.7	17.0
150	45.7	20	6.1	91.5	1.7	65.4	19.9
200	61.0	20	6.1	91.3	1.25	85.8	26.2
250	76.2	20	6.1	89.0	0.98	107.9	32.9

Table 5. Field Data for VES 2 (4/2/83)

AB/2		MN		I (ma)	V (mv)	Ra	
(ft)	(m)	(ft)	(m)			(ohm-ft)	(ohm-m)
2.5	0.8	2	0.6	100	5250	433.0	132.0
5	1.5	2	0.6	109	1210	418.5	127.4
7.5	2.3	2	0.6	121	540	387.3	118.0
10	3.0	2	0.6	125	290	360.8	110.0
15	4.6	2	0.6	116	111	336.7	102.7
20	6.1	2	0.6	118	55	292.1	89.0
30	9.1	2	0.6	118	21	251.3	76.5
40	12.2	2	0.6	105	11	263.1	80.2
50	15.2	2	0.6	108	8	290.8	88.7
70	21.3	2	0.6	105	4.9	359.1	109.4
100	30.5	2	0.6	118	3.5	465.9	142.0
100	30.5	4	1.2	118	7.2	479.0	146.0
150	45.7	4	1.2	138	5.1	653.0	199.0
200	61.0	4	1.2	140	3.7	830.2	253.0

Table 6. Field Data for VES 3 (4/15/83)

AB/2		MN		I (ma)	V (mv)	Ra	
(ft)	(m)	(ft)	(m)			(ohm-ft)	(ohm-m)
2.5	0.8	1	0.3	141	185	24.7	7.5
3	0.9	1	0.3	140	120	23.6	7.2
4	1.2	1	0.3	142	65	22.7	6.9
5	1.5	1	0.3	140	41	22.8	6.9
6	1.8	1	0.3	140	28	22.5	6.9

Table 6. (continued)

AB/2		MN		I (ma)	V (mv)	Ra	
(ft)	(m)	(ft)	(m)			(ohm-ft)	(ohm-m)
7.5	2.3	1	0.3	141	18	22.5	6.9
10	3.0	1	0.3	142	9	19.9	6.1
12.5	3.8	1	0.3	145	5.0	16.9	5.2
15	4.6	1	0.3	146	3.9	18.9	5.8
20	6.1	1	0.3	148	2.5	21.2	6.5
25	7.6	1	0.3	142	1.65	22.8	6.9
25	7.6	2	0.6	144	3.3	22.5	6.9
30	9.1	2	0.6	143	2.45	24.2	7.4
40	12.2	2	0.6	141	1.70	30.3	9.2
50	15.2	2	0.6	135	1.2	34.9	10.6
50	15.2	4	1.2	132	3.6	53.5	16.3
60	18.3	4	1.2	138	3.0	61.4	18.7
75	22.9	4	1.2	135	2.4	78.5	23.9

Table 7. Field Data for VES 4 (4/22/83)

AB/2		MN		I (ma)	V (mv)	Ra	
(ft)	(m)	(ft)	(m)			(ohm-ft)	(ohm-m)
2.5	0.8	1	0.3	96	10500	2061.7	628.4
3	0.9	1	0.3	98	8000	2244.0	684.0
4	1.2	1	0.3	95	5100	2656.3	809.6
5	1.5	1	0.3	87	3200	2859.9	871.7
6	1.8	1	0.3	89	2500	3154.8	961.6
8	2.4	1	0.3	90	1550	3449.2	1051.3

Table 7. (continued)

AB/2		MN		I	V	Ra	
(ft)	(m)	(ft)	(m)	(ma)	(mv)	(ohm-ft)	(ohm-m)
10	3.0	1	0.3	88	1050	3739.1	1139.7
12.5	3.8	1	0.3	96	760	3879.9	1182.6
15	4.6	1	0.3	92	520	3990.9	1216.4
20	6.1	1	0.3	85	260	3841.4	1170.9
25	7.6	1	0.3	88	160	3568.6	1087.7
30	9.1	1	0.3	92.5	120	3667.0	1117.7
32	9.8	1	0.3	84	85	3254.5	992.0
40	12.2	1	0.3	87	52	3003.9	915.6
50	15.2	1	0.3	92	32.5	2774.2	845.6
60	18.3	1	0.3	98	22.5	2596.4	791.4
80	24.4	1	0.3	82	10.08	2471.5	753.3
100	30.5	1	0.3	82	6.2	2375.3	724.0
125	38.1	1	0.3	82	4.0	2394.5	729.8
125	38.1	4	1.2	83	15.8	2335.5	711.9
150	45.7	4	1.2	79	9.8	2191.8	668.1
200	61.0	4	1.2	51	2.6	1601.4	488.1
225	68.6	4	1.2	69	4	2304.8	702.5
250	76.2	4	1.2	79	4	2485.3	757.5
275	83.8	4	1.2	95	4	2500.7	762.2



Table 8. Field Data for VES 5 (4/22/83)

AB/2		MN		I	V	Ra	
(ft)	(m)	(ft)	(m)	(ma)	(mv)	(ohm-ft)	(ohm-m)
2.5	0.8	1	0.3	99	8200	1561.3	475.9
3	0.9	1	0.3	98	6100	1711.1	521.5
4	1.2	1	0.3	95	3850	2005.3	611.2
5	1.5	1	0.3	98	2900	2300.9	701.3
6	1.8	1	0.3	92	2050	2502.6	762.8
8	2.4	1	0.3	96	1300	2712.1	826.6
10	3.0	1	0.3	100	940	2945.7	897.8
12.5	3.8	1	0.3	100	610	2989.5	911.2
15	4.6	1	0.3	100	420	2965.5	903.9
20	6.1	1	0.3	100	235	2951.3	899.6
25	7.6	1	0.3	85	125	2886.3	879.7
30	9.1	1	0.3	98	95	2740.1	835.2
40	12.2	1	0.3	86	40	2337.6	712.5
50	15.2	1	0.3	89	24	2117.7	645.5
60	18.3	1	0.3	92	16	1966.8	599.5
80	24.4	1	0.3	87	7.8	1802.6	549.4
90	27.4	1	0.3	78	5.15	1680.1	512.1
100	30.5	1	0.3	92	4.8	1639.1	499.6
125	38.1	1	0.3	85	2.6	1501.5	457.7
125	38.1	4	1.2	85	10.1	1457.8	444.3
150	45.7	1	0.3	81	1.7	1483.5	452.2
150	45.7	4	1.2	81	7.0	1526.9	465.4
175	53.3	4	1.2	83	5.4	1564.7	476.9
200	61.0	1	0.3	92	1.15	1570.8	478.8

Table 8. (continued)

(ft)	AB/2	(ft)	MN	I	V	a	
	(m)		(m)			(ohm-ft)	(ohm-m)
200	61.0	4	1.2	92	4.75	1621.9	494.4
250	76.2	4	1.2	91	3.6	1941.8	591.9
275	83.8	4	1.2	122	4.4	2142.0	652.9

Table 9. Field Data for VES 6 (4/23/83)

(ft)	AB/2	(ft)	MN	I	V	Ra	
	(m)		(m)			(ohm-ft)	(ohm-m)
2.5	0.8	1	0.3	160	245	28.9	8.8
3	0.9	1	0.3	160	165	28.4	8.7
3.5	1.1	1	0.3	152	119	29.5	9.0
4	1.2	1	0.3	152	87	28.3	8.6
5	1.5	1	0.3	160	59	28.7	8.7
6	1.8	1	0.3	158	41	29.1	8.9
7	2.1	1	0.3	157	29.5	28.8	8.8
8	2.4	1	0.3	158	21.5	27.3	8.3
10	3.0	1	0.3	160	13	25.5	7.8
12.5	3.8	1	0.3	159	7.7	23.7	7.2
15	4.6	1	0.3	160	5.2	23.0	7.0
17.5	5.3	1	0.3	160	3.95	23.7	7.2
20	6.1	1	0.3	160	3.15	24.7	7.5
20	6.1	4	1.2	160	13.5	26.2	8.0
25	7.6	1	0.3	160	2.05	25.2	7.7
25	7.6	4	1.2	160	8.85	27.0	8.2

Table 9. (continued)

(ft)	AB/2	(ft)	MN	I (ma)	V (mV)	Ra	
	(m)		(m)			(ohm-ft)	(ohm-m)
30	9.1	4	1.2	160	6.9	30.4	9.3
40	12.2	4	1.2	154	4.4	35.8	10.9
45	13.7	4	1.2	140	3.40	38.6	11.8
50	15.2	4	1.2	115	2.3	39.2	11.9
60	18.3	4	1.2	132	2.1	44.9	13.7
70	21.3	4	1.2	112	1.5	51.5	15.7
75	22.9	4	1.2	120	1.55	57.0	17.4
80	24.4	4	1.2	112	1.4	62.8	19.1
90	27.4	4	1.2	75	0.85	72.1	22.0
100	30.5	4	1.2	111	1.17	82.8	25.2

## APPENDIX D. AB Rectangle Mapping Field Data

Table 10. Field Data for ABR 1 (4/22/83)

AB/2 = 175ft (53.34m)

0,0 is ABR center and positive X is towards B in figure 18.

Coordinates		MN		I	V	Ra	
X(ft)	Y(ft)	(ft)	(m)	(ma)	(mv)	(ohm-ft)	(ohm-m)
-10	10	4	1.2	82	5.0	1459.4	444.8
-5	10	4	1.2	82	5.8	1705.3	519.8
0	10	4	1.2	82	5.2	1532.6	567.1
5	10	4	1.2	82	5.5	1617.1	492.9
10	10	4	1.2	82	5.6	1634.5	498.2
-10	5	4	1.2	82	4.5	1308.5	398.8
-5	5	4	1.2	82	5.8	1699.0	517.9
0	5	4	1.2	82	6.1	1791.2	546.0
5	5	4	1.2	82	5.3	1552.5	473.2
10	5	4	1.2	82	5.3	1541.1	469.7
-10	0	4	1.2	85	4.7	1316.8	401.4
-5	0	4	1.2	80	6.25	1874.3	571.3
0	0	4	1.2	83	5.4	1564.7	476.9
5	0	4	1.2	80	4.4	1319.5	402.2
10	0	4	1.2	85	5.3	1484.9	452.6
-10	-5	4	1.2	83	5.5	1580.0	481.6
-5	-5	4	1.2	82	5.5	1611.1	491.1
0	-5	4	1.2	83	4.8	1392.5	424.4
5	-5	4	1.2	82	4.8	1406.1	428.6

Table 10. (continued)

Coordinates		MN		I	V	Ra	
X(ft)	Y(ft)	(ft)	(m)	(ma)	(mv)	(ohm-ft)	(ohm-m)
10	-5	4	1.2	82	4.8	1395.8	425.4
-10	-10	4	1.2	83	5.5	1586.1	483.4
-5	-10	4	1.2	82	5.5	1617.1	492.9
0	-10	4	1.2	83	4.4	1281.2	390.5
5	-10	4	1.2	82	4.5	1323.1	403.3
10	-10	4	1.2	82	5.0	1459.4	444.8

Table 11. Field Data for ABR 2 (4/15/83)

AB/2 = 30ft (9.1m)

0,0 is ABR center and positive X is towards B in figure 19.

Coordinates		MN		I	V	Ra	
X(ft)	Y(ft)	(ft)	(m)	(ma)	(mv)	(ohm-ft)	(ohm-m)
-10	10	2	0.6	145	2.9	26.6	8.1
-5	10	2	0.6	145	1.8	19.4	5.9
0	10	2	0.6	145	2.2	25.1	7.7
5	10	2	0.6	143	2.7	29.5	9.0
10	10	2	0.6	145	3.0	27.5	8.4
-10	5	2	0.6	145	4.2	31.4	9.6
-5	5	2	0.6	145	2.7	25.4	7.7
0	5	2	0.6	145	2.6	26.4	8.0
5	5	2	0.6	145	3.3	31.0	9.4
10	5	2	0.6	145	2.5	18.7	5.7

Table 11. (continued)

Coordinates		MN		I	V	Ra	
X (ft)	Y (ft)	(ft)	(m)	(ma)	(mv)	(ohm-ft)	(ohm-m)
-10	0	2	0.6	145	4.6	31.8	9.7
-5	0	2	0.6	146	3.3	29.3	8.9
0	0	2	0.6	145	2.9	28.0	8.5
5	0	2	0.6	145	3.7	33.1	10.1
10	0	2	0.6	145	3.3	22.8	6.9
-10	-5	2	0.6	145	3.85	28.8	8.8
-5	-5	2	0.6	148	4.6	42.4	12.9
0	-5	2	0.6	145	4.6	46.7	14.2
5	-5	2	0.6	143	2.7	25.8	7.9
10	-5	2	0.6	145	2.8	20.9	6.4
-10	-10	2	0.6	145	2.6	23.9	7.3
-5	-10	2	0.6	145	3.7	39.9	12.2
0	-10	2	0.6	145	3.8	43.4	13.2
5	-10	2	0.6	145	2.2	23.7	7.2
10	-10	2	0.6	143	2.3	21.4	6.5

Table 12. Field Data for ABR 3 (4/23/83)

AB/2 = 45ft (13.7m)

0,0 is ABR center and positive X is towards B in figure 20.

Coordinates		MN		I	V	Ra	
X(ft)	Y(ft)	(ft)	(m)	(ma)	(mv)	(ohm-ft)	(ohm-m)
-10	10	4	1.2	140	3.4	36.6	11.2
-5	10	4	1.2	140	4.2	49.6	15.1
0	10	4	1.2	140	2.3	28.0	8.5
5	10	4	1.2	140	2.22	26.2	8.0
10	10	4	1.2	140	2.15	23.1	7.0
-10	5	4	1.2	140	4.9	49.0	14.9
-5	5	4	1.2	140	4.2	46.8	14.3
0	5	4	1.2	140	2.55	29.5	9.0
5	5	4	1.2	140	2.35	26.2	8.0
10	5	4	1.2	140	2.35	23.5	7.2
-10	0	4	1.2	140	5.4	52.7	16.1
-5	0	4	1.2	140	4.7	51.3	15.6
0	0	4	1.2	140	3.4	38.6	11.8
5	0	4	1.2	140	2.6	28.4	8.7
10	0	4	1.2	140	2.6	25.4	7.7
-10	-5	4	1.2	140	6.7	67.0	20.4
-5	-5	4	1.2	140	4.4	49.0	14.9
0	-5	4	1.2	140	3.0	34.7	10.6
5	-5	4	1.2	140	3.1	34.6	10.5
10	-5	4	1.2	140	2.55	25.5	7.8
-10	-10	2	0.6	140	2.4	51.7	15.8

Coordinates		MN		I	V	Ra	
X(ft)	Y(ft)	(ft)	(m)	(ma)	(mv)	(ohm-ft)	(ohm-m)
-5	-10	2	0.6	140	2.2	52.1	15.9
0	-10	4	1.2	140	2.15	26.2	8.0
5	-10	4	1.2	140	2.18	25.8	7.9
10	-10	4	1.2	140	2.65	28.5	8.7

Table 13. Field Data for ABR 4 (4/23/83)

AB/2 = 60ft (18.3m)

0,0 is ABR center and positive X is towards B in figure 21.

Coordinates		MN		I	V	Ra	
X(ft)	Y(ft)	(ft)	(m)	(ma)	(mv)	(ohm-ft)	(ohm-m)
-10	10	4	1.2	130	2.0	42.0	12.8
-5	10	4	1.2	130	2.55	56.7	17.3
0	10	4	1.2	130	1.48	33.5	10.1
5	10	4	1.2	130	1.37	30.4	9.3
10	10	4	1.2	130	1.2	25.2	7.7
-10	5	4	1.2	130	2.75	55.6	16.9
-5	5	4	1.2	130	2.5	53.8	16.4
0	5	4	1.2	130	1.55	34.0	10.4
5	5	4	1.2	130	1.35	29.0	8.8
10	5	4	1.2	130	1.28	25.9	7.9
-10	0	4	1.2	130	3.0	59.9	18.3
-5	0	4	1.2	130	2.85	60.6	18.5
0	0	4	1.2	130	2.08	45.2	13.8



Table 13. (continued)

Coordinates		MN		I	V	Ra	
X(ft)	Y(ft)	(ft)	(m)	(ma)	(mv)	(ohm-ft)	(ohm-m)
5	0	4	1.2	130	1.5	31.9	9.7
10	0	4	1.2	130	1.4	28.0	8.5
-10	-5	4	1.2	130	3.9	78.9	24.0
-5	-5	4	1.2	130	2.65	57.0	17.4
0	-5	4	1.2	130	1.65	36.2	11.0
5	-5	4	1.2	130	2.5	53.8	16.4
10	-5	4	1.2	130	1.45	29.3	8.9
-10	-10	2	0.6	130	1.35	56.7	17.3
-5	-10	2	0.6	130	1.42	63.1	19.2
0	-10	4	1.2	130	1.4	31.7	9.7
5	-10	4	1.2	130	1.4	31.1	9.5
10	-10	4	1.2	130	1.55	32.5	9.9